Pacific Northwest
NATIONAL LABORATORY

PNNL-34860

Design and Development of a High Fidelity Cyber-Physical Testbed

September 2023

Rohit Jinsiwale
Manisha Maharjan
Priya Mana
Aditya Ashok
Tamara Becejac
Scott Harpool
William Hofer
Arcadio Vielma
Gustavo Gloria
Thomas Edgar

U.S. DEPARTMENT OF ENERGY

Prepared for the U.S. Department of Energy
under Contract DE-AC05-76RL01830

DISCLAIMER

PACIFIC NORTHWEST NATIONAL LABORATORY
operated by
BATTELLE
for the
UNITED STATES DEPARTMENT OF ENERGY
under Contract DE-AC05-76RL01830

Printed in the United States of America

Available to DOE and DOE contractors from the Office of Scientific and Technical Information,
P.O. Box 62, Oak Ridge, TN 37831-0062
www.osti.gov
ph: (865) 576-8401
fax: (865) 576-5728
email: reports@osti.gov

Available to the public from the National Technical Information Service
5301 Shawnee Rd., Alexandria, VA 22312
ph: (800) 553-NTIS (6847)
or (703) 605-6000
email: info@ntis.gov
Online ordering: http://www.ntis.gov

PNNL-34860

Design and Development of a High Fidelity Cyber-Physical Testbed

September 2023

Rohit Jinsiwale
Manisha Maharjan
Priya Mana
Aditya Ashok
Tamara Becejac
Scott Harpool
William Hofer
Arcadio Vielma
Gustavo Gloria
Thomas Edgar

Prepared for
the U.S. Department of Energy
under Contract DE-AC05-76RL01830

Pacific Northwest National Laboratory
Richland, Washington 99354

Abstract

In order to ensure that future critical infrastructure systems are resilient to various types of such advanced and persistent threats, it is important to develop and integrate tailored solutions that holistically address cyber-attack detection and mitigation in a timely manner such that adverse system impacts that impact a large population are avoided. Further, it is essential to create environments that allow control, protection and communication to exist within a realistic environment to analyze the effects of adverse conditions and system operating modes. This project aims to establish a high-fidelity testbed environment for modeling and simulating a single microgrid all the way up to a network of microgrids along with baseline controls, protection, and associated cyber communication. This is an important activity because accurately modeling and simulating the various power-electronics-based DERs and loads in a microgrid is critical to adequately capturing their behaviors over a wide range of off-normal conditions, as well as to evaluate the resilience of the system using the developed controls.

The work presented in this report focuses on the process of building this high-fidelity testbed and the associated experimentation it enables. The model enables the creation of high-fidelity use cases and associated datasets that have been used extensively within the initiative to study resilience and support novel control development and prototyping. The work heavily leverages existing capability that is part of the high-fidelity cyber-physical system experimentation lab to create a power hardware-in-the-loop setup. The report also details the creation of an automated model building platform that can enable high-fidelity real-time models to be built without much effort allowing existing low-fidelity models to be analyzed in higher fidelity. Lastly, the report also discusses efforts center around scaling to large complex power system models to make the experimentation more effective.

Acknowledgments

This research was supported by the National Security Mission Seed, under the Laboratory Directed Research and Development (LDRD) Program at Pacific Northwest National Laboratory (PNNL). PNNL is a multi-program national laboratory operated for the U.S. Department of Energy (DOE) by Battelle Memorial Institute under Contract No. DE-AC05-76RL01830.

Contents

Figures

Tables

1.0 Background and Motivation

Over the last decade, there has been a tremendous increase in the penetration of renewable generation and Distributed Energy Resources (DERs) across the bulk transmission and distribution systems all the way down to consumer level DERs. These DERs are primarily interfaced through power electronics-based converters that are switched at high frequencies. Consequently, there is an increasing reliance on fast acting controls to ensure the stability, reliability, and resilience of the future grid across a range of normal and off-normal scenarios. Further, as newer DERs come online and the overall generation mix evolves, it is essential to capture their interactions with existing synchronous machine controls as well as the behavior of protection elements at high-fidelity. This need for extensively studying DERs and their performance before their grid integration through the use of high-fidelity, electromagnetic transients (EMT) simulation tools is well-recognized in recent industry standards and technical reports.

Microgrids are becoming an increasingly common solution to improve system resilience at the distribution level. Owing to embedded distributed generation and the ability to operate in grid-connected and islanded modes, microgrids serve as the most interesting use case to analyze transient phenomenon at high fidelity. Increased levels of renewable penetration introduce rapidly changing dynamics. This introduces emergent and ensemble behaviors on the system under adverse conditions. It is critical to study the behavior of future grids under a variety of adverse conditions and enable prototyping/evaluation of the new control methodologies for enhancing reliability and resilience.

1.1 Need for Cyber-Physical Testbeds

Complex grid systems including microgrids are typically interfaced with controllers and protection devices that need to be tuned to respond correctly in grid-connected and islanded modes. This process requires physical devices such as relays and controllers to be interfaced with a model that can be simulated in real-time to analyze and tune these devices. Simulating large complex system with all the associated controls, protection elements in real-time is challenging due to the associated computational burden. Microgrids with a high penetration of power electronics based DERs as well as dynamic loads (variable frequency drives, EVs, etc.) incorporate different types and levels of associated controls, protection, and communication. Prior efforts focusing on modeling/simulation of microgrids typically abstract one of the following the controls, protection or communication depending on the focus of the experiment and do not explicitly consider the interactions and their impact on the performance under various adverse conditions. There are a few prior efforts that leverage specialized test ranges, campus level microgrids, or high-fidelity models to perform targeted experiments on small scale systems [1]–[6].

Cyber-physical testbeds are extremely essential in providing realistic environments for replicating real-world critical infrastructure systems to perform various experimental studies for prototyping, validation, as well as training and educational activities. In this context, to study and understand the behaviors of microgrid systems and subsystems at scale over a wide-range of off-normal conditions, a high-fidelity cyber-physical testbed environment is essential. Specifically, it is essential to develop high-fidelity component and system models to simulate the various power electronics based DERs such as PV inverters, battery energy storage systems, and dynamic loads such as induction motor loads with Variable Frequency Drives (VFDs), etc., In addition, it is critical that the testbed environment also includes the associated controls, protection, and communication elements appropriately so that the overall resilience of the microgrid systems can

be accurately studied and quantified. Cyber-physical testbeds are vital to accurately assess the performance and resilience of these systems under a wide range of adverse conditions (faults and cyber-attacks).

1.1.1 Necessary components of a viable testbed

A cyber-physical testbed can take on many forms depending on the use cases of interest, desired level of fidelity and reconfigurability desired. Typically, cyber-physical testbeds encompass three key layers from an architectural standpoint [7]. The first of these is a physical layer that emulates the physics of the grid being modelled. This is typically achieved by using power system modelling engines or by creating a scaled version of the test system in the real-world. The second of these is the communication layer. This layer characterizes all the network flows and interactions between various controllers, data acquisition systems and quantifies control actions exerted on the system. Lastly, the information and control layer models supervisory control schemes and captures the algorithms issuing control actions to the power system. Conceptually, these three layers are vital to creating a complete cyber-physical testbed. Figure 1 characterizes this conceptual architecture.

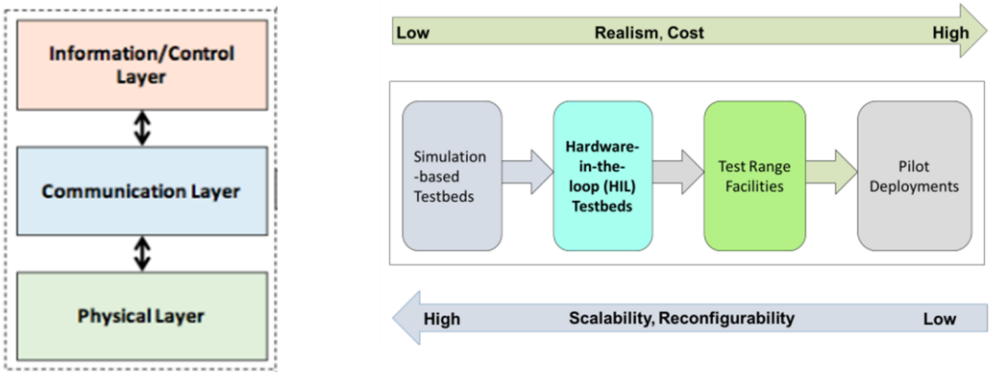

Figure 1: Conceptual Architecture of cyber-physical testbeds (left), Possible implementations of a cyber-physical testbed (right)

These three layers summarized above can be realized in a variety of ways. Figure 1 depicts a range of example testbeds. Large systems may be replicated purely in a simulation-based testbed to accurately model the dynamics of the system. While this leads to a highly configurable and scalable model framework it limits the realism that can be embedded into possible experiments. On the other hand, a real-world power system can be constructed to serve as a testbed to incorporate the highest amount of realism, but it fails to be reconfigurable to be put through rigorous experimentation. A hardware-in-the-loop (HIL) approach enables high-fidelity reconfigurable simulation models to be integrated with real-world controllers and protection devices to provide a reasonable balance between realism, fidelity and reconfigurability.

1.1.2 Cyber-physical testbed design

As summarized in the previous subsection, there are numerous ways to realize cyber-physical testbeds depending on the specific experimentation requirements, required repeatability, fidelity levels, scalability, flexibility, and realism required. The process for defining a testbed architecture

is focused on realizing these attributes for the specific use cases in question. For distribution grids with microgrids it is key to study the impact of high DER penetration, characterize the vulnerability of such structures and evaluate impact and counter measures under adverse conditions. These use cases further define specific requirements for the testbed.

Owing to embedded distributed generation and the ability to operate in grid-connected and islanded modes, microgrids serve as the most interesting use case to analyze transient phenomenon at high fidelity. Moreover, microgrids are typically interfaced with microgrid controllers and protection devices that need to be tuned to respond correctly in grid-connected and islanded modes. This process requires physical devices such as relays and controllers to be interfaced with a model that can be simulated in real-time to analyze and tune these devices.

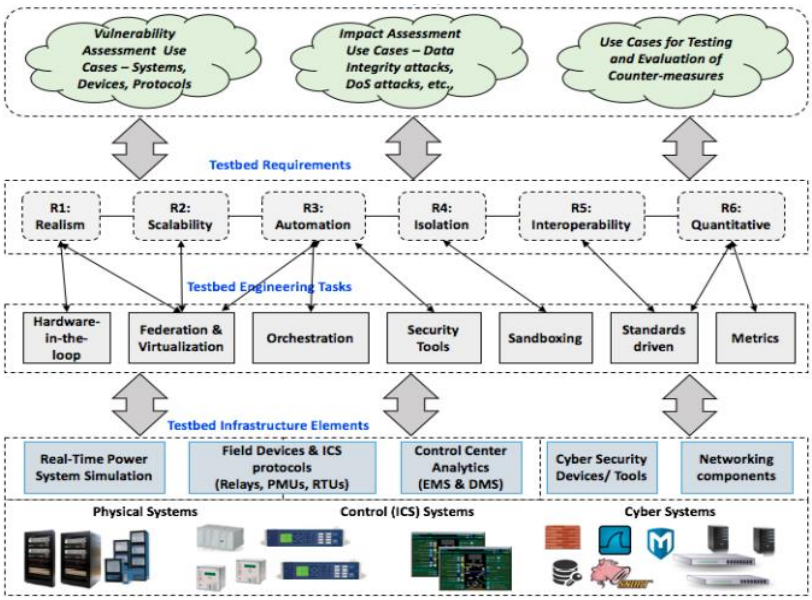

Figure 2: Cyber-Physical Testbed Design Process

By defining these attributes specific hardware components, simulation engines, network requirements and attack tools can be identified. Figure 2 provides and overview of the testbed design process for the use cases that are essential to this report's scope. High-Fidelity simulations will be conducted on OPAL-RT simulators using HYPERSIM [8] and eFPGASim [9] as modelling tools. A variety of multi-vendor field devices such as RTUs, protective relays and controllers will be integrated into this setup to bring realism to microgrid-based use cases. Attack scripting tools (MITRE Caldera), open platform communication (servers) and network equipment are integrated to support network building and emulation.

This project will integrate and enhance PNNL's existing simulation, emulation, and hardware capabilities that have been created through prior initiatives such as the following testbeds:

• powerNET & cyberNET testbeds (high-fidelity cyber-physical system experimentation lab [10])

• Building controls lab [11]

• Energy storage lab [12]

1.2 Research Design and Methodology

The report will detail the design of building blocks needed to instantiate high-fidelity models and the architecture implemented to realize a high-fidelity testbed for experimentation. The developed testbed models will be integrated along with their baseline controls, protection elements, and setup to communicate with each other similar to a real-world environment. Once the model integration is complete, it will be used to perform a series of experiments to generate realistic datasets for a range of use case scenarios.

Figure 3 shows a conceptual architecture of the cyber-physical testbed environment that we plan to use to generate high-fidelity observational datasets as well as to validate the developed controls for resilient microgrids as a part of the initiative. The testbed environment consists of a variety of simulators to enable accurate, multi-fidelity modeling and simulation of the microgrid. To perform a high-fidelity, real-time simulation of a large microgrid model using HYPERSIM and eFPGASim, we utilize a real-time simulator with adequate computational capability in terms of available CPU cores to split the various components within the microgrid model appropriately, as well as adequate FPGA resources to model the detailed switching actions of power electronics components and their converters. Opal-RT simulator hardware with Input/Output (IO) modules can support power hardware in the loop experimentation with real DERs.

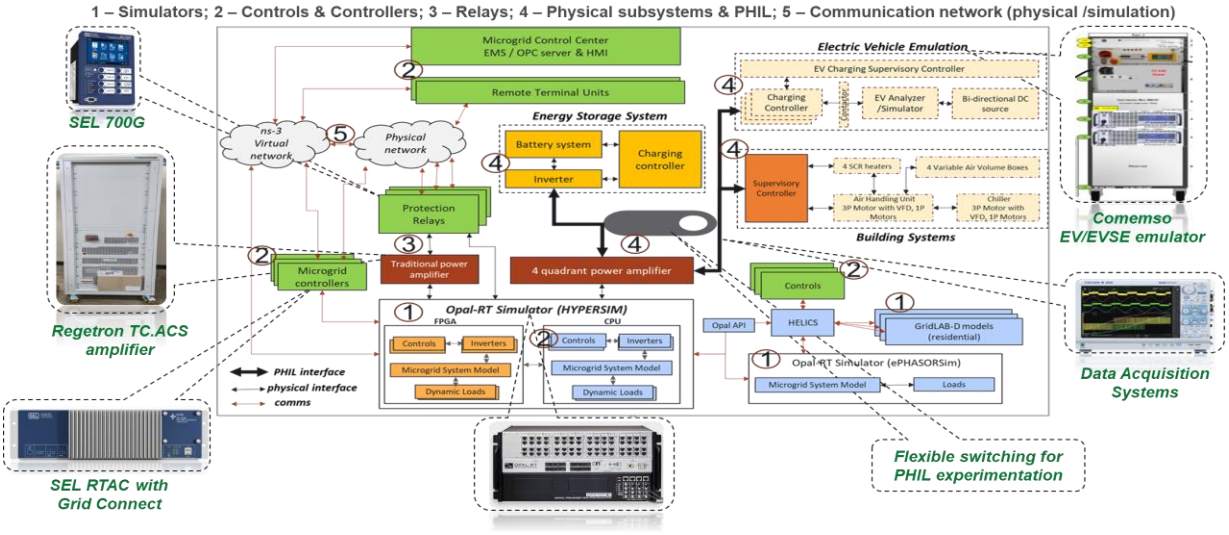

Figure 3: High-Fidelity Cyber-Physical Testbed Architecture

The architecture also provides flexibility to perform rapid control prototyping by offering multiple ways (eFPGASim, prototype boards, software) to implement the control algorithms on real-world prototype controllers and evaluate their performance in effectively controlling the power electronic resources in the microgrid under various types of adversities. To accurately capture the behavior of protection components, the testbed architecture consists of several protection relays that are coupled to the real-time microgrid simulator either directly or through power amplifiers. The protective relays will be configured to communicate with remote terminal units (RTUs) to send the available measurements and receive control commands. A bi-directional four quadrant power

amplifier allows the integration of multiple types of DER subsystems as well as build loads in the SEB Annex through power hardware in the loop experimentation. A flexible switching arrangement enables easy interconnection of these hardware resources into our testbed environment to study their behaviors under various conditions at high fidelity. A communication network is modeled to simulate the underlying communication infrastructure properly while including the various underlying communication protocol behaviors as well as the network behaviors including bandwidth, latency characteristics, etc.

1.3 Report Organization

The remainder of this report is laid out in sections as follows. Section 2 explores challenges with modelling distribution systems with microgrids in high-fidelity. The section captures the challenges with leveraging multiple CPU cores to realize large high-fidelity models and proposes a new decoupling framework that serves to enable high-fidelity simulations detailed in this report. Section 3 details the developed cyber-physical testbed that allows multiple microgrids to be instantiated and analyzed as well as a cyber layer that can support a variety of attack modelling. The section also explores studies that were conducted to benchmark the model and accuracy comparisons with benchmarked GridLAB-D models [13]. The section also explores accuracy validation for the novel decoupling approach proposed in this work. To effectively utilize the developed testbed, it is vital to create a pipeline that can automate scenario creating and recreate specific conditions in a repeatable manner. To this end, Section 4 explores a pipeline that was developed to enable orchestration of scenarios to enable prototyping and validation of novel controls. Section 5 focuses on the datasets that can be generated from the developed testbed. The section explores the nature and fidelity of the datasets captured. Section 6 details the cyber-physical use case and the associated datasets that were generated to analyze the system and characterize resilience, attack vulnerability and system operating modes. Section 7 then focuses on the roadmap to developing larger and more complex models to conduct further studies in DER-heavy microgrid systems. The section captures the challenges with developing high-fidelity models at scale and proposes a few approaches to realize larger high-fidelity models. Finally, Section 8 explores the impact the work discussed in this report has had.

2.0 High Fidelity Experimentation Methods

This need for extensively studying DERs and their performance before their grid integration through the use of high-fidelity, electromagnetic transients (EMT) simulation tools is well-recognized in recent industry standards and technical reports [14].Simulating large complex system with all the associated controls, protection elements in real-time is challenging due to the associated computational burden. Typically, real-time simulators achieve this scalability by decoupling the system model into sections that can run independently on individual cores of a simulator. While decoupling the system works well without degrading simulation accuracy for transmission system models with long lines, it is challenging for microgrids/distribution systems with short lines.

2.1 Challenges with large scale model simulation

Traditional distribution systems were routinely analyzed using phasor domain or quasi-steady state approaches. However, modern distribution networks containing microgrids are significantly more complex and need to be analyzed in greater detail to ensure safe operation. For instance, a distribution system with multiple microgrids may have to be analyzed to ensure safe operation when all the microgrids are islanded, grid-connected or any combinatorial possibility in between those states. To this end, the level of fidelity and accuracy varies on the simulation approach taken. Two main types of approaches exist to realizing large system simulation models and are highlighted in Figure 4. Each of these approaches will be detailed in the next two subsections.

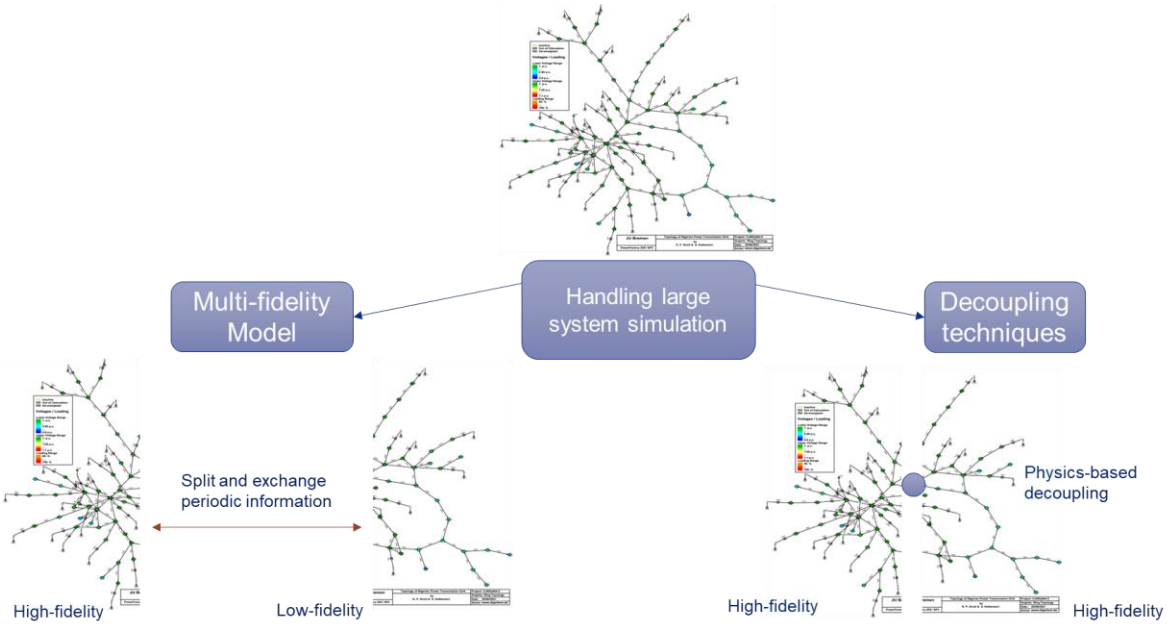

Figure 4: Large Scale Model Simulation Techniques

2.1.1 Multi-fidelity Approaches

While DERs operate extremely fast, other parts of the system may react slowly to changing conditions. Some approaches leverage this difference to separate the system into factions where DERs and fast switching devices are simulated at lower time steps in an electromagnetic transient (EMT) solver, while the rest of the system is simulated at time-steps of a higher order of magnitude in a transient system analysis (TSA) package, thereby reducing the net computational burden [15]. A TSA package relies on a phasor domain (positive sequence) model of a part of the system with slow dynamics. The interface between the two domains is typically bridged by using a Norton and Thevenin equivalent for either domain to approximate the rest of the system at the interface. These equivalents are synchronized at regular intervals; often based on the slower TSA time-step. Figure 5 shows the general configuration of such a scheme.

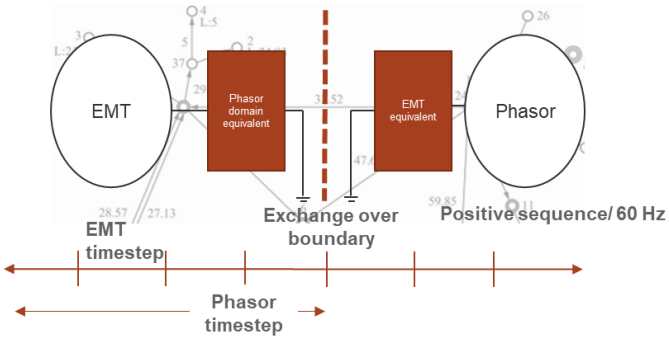

Figure 5: Multi-fidelity approach leveraging EMT and phasor domains

This means that an event like a fault or topology change in either domain is only synchronized across the boundary at slow intervals reducing the accuracy. The phasor domain seldom models the frequency dynamics of synchronous machines on the grid causing a loss of accuracy and a failure to observe the effect of fast dynamics on machine stability. Moreover, a positive sequence equivalent for three phase quantities does not capture the effect of harmonics introduced by DERs at the boundary between the two domains. It can be noted that certain approaches [16], [17] involve incorporating some dynamic states associated with synchronous swing dynamics, however, the accuracy errors due to synchronization delays still persist. These shortcomings make it challenging to accurately analyze fast phenomenon, tune protection devices, and assess system stability using these approaches.

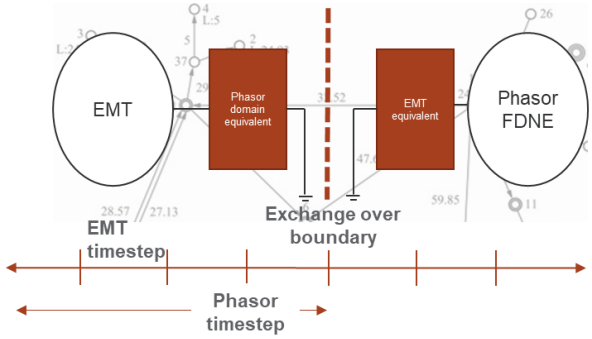

Figure 6: Multi-fidelity approach leveraging a frequency equivalent in the phasor domain

Another approach proposed in [8] relies on developing a linear approximation of the TSA system for different points on the frequency spectrum to improve some accuracy. Figure 6 shows a

general realization of such an approach. Such Frequency Dependent Network Equivalents (FDNE) are typically derived in advance and typically do not reflect topology changes. Moreover, FDNEs necessitate the use of a higher degree transfer function which makes the hybrid approach susceptible to numerical instability. FDNE approaches also become computationally burdensome when a larger number of boundaries are considered, which may happen in meshed topologies. Another key assumption in such hybrid simulation approaches is that the EMT-side boundary is well-damped. This assumption is essential to ensure that the three phase quantities being transformed to phasor equivalents don't have high frequency components that can cause numerical issues [18]. The relaxation scheme used at the boundary also has impacts on convergence characteristics of hybrid simulations [19]. This implies that hybrid simulation schemes are sensitive to the placement of the boundary, the boundary relaxation scheme and limit the phenomenon that can be analyzed. While these approaches succeed in reducing computational burdens significantly, simulation accuracy is compromised when using these approaches [20]. Also, in both approaches, significant information about harmonics and transients is lost owing to the synchronization delays. Capturing these factors accurately in the simulation are extremely critical to ensuring that safe and reliable operation of microgrids is achieved.

The shortcomings of the above approaches can be addressed by identifying mechanisms to simulate distribution systems with a unified time-step across the entire topology, thereby ensuring the highest amount accuracy and fidelity. Real-time simulation-based approaches allow analysis of power systems with small time-steps on dedicated digital simulators. However, depending on the size of the system and the number of nonlinear components, the associated computations may become challenging without decoupling the system and leveraging its multi-core parallel computational capabilities. Multicore computations involve strategically decoupling the system into multiple segments and simulating them in parallel to enable computation times that are still under the required timestep. The location and the design of these decoupling points is critical to ensuring accuracy while introducing minimal additional error.

2.1.2 Decoupling Techniques

As opposed to the aforementioned multi-fidelity approaches, physics-based decoupling approaches utilize the unique structure of the power system's states or delays across passive elements as the basis for decoupling the system and using multi-core setups to simulate them in high-fidelity. A few decoupling approaches are observed in relevant literature: (1) Bordered Block Diagonal (BBD) structure-based state delay, (2) V/V and V/I methods, (3) Transmission line propagation delay-based decoupling. Each of these approaches enables the use of multiple compute cores to split the computational burden associated with simulating large systems.

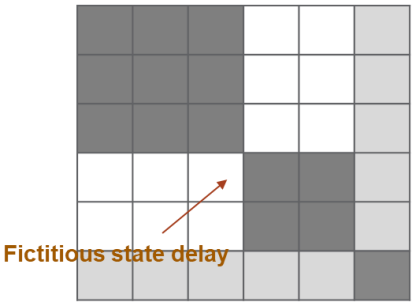

Figure 7: Block Bordered Diagonal (BBD) based state delay

A power system solver typically deals with solving a Jacobian matrix associated with the impedance parameters of the network. This Jacobian is a function of the numerical integration

method used. Implicit Trapezoidal Method (ITM) is a popular numerical method. Jacobians constructed using ITM approaches typically follow a BBD structure. Numerous techniques have been proposed to explore the sparsity of BBD matrices to find state variables that can be delayed by one time-step in computation [21]. Figure 7 shows an illustration of such state variables in typical sparse matrices. This allows a larger coupled network to be decoupled around these delayed state variables and solved. However, it is important to note that these delays are fictitious in nature and do not actually reference any physical propagation delays within the network. Additionally, the process of identifying these state variables is complex and requires analysis. In case of distribution networks with microgrids, it becomes extremely challenging to compute Jacobian matrices for all possible configurations and further process them to identify these system variables. Moreover, the approach works well for transmission systems where the Jacobian is inherently more decoupled due to high X/R ratios. Due to lower X/R ratios observed in distribution systems this approach becomes infeasible for microgrid studies.

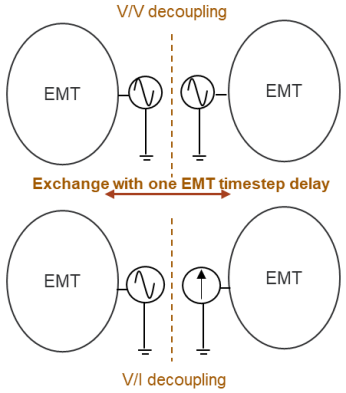

Figure 8: V/V and V/I Decoupling Schemes

V/V and V/I decoupling schemes are highly similar to the hybrid simulation approach summarized in the previous subsection with the exception that all the decoupled sections are simulated using the same EMT scheme. This means that the interface between the decoupled section will involve two voltage sources for a V/V scheme (individually interfaced to each decoupled section) or a voltage and current source for a V/I scheme. The sources exchange information from a prior time-step to create an equivalent for the rest of the system for each domain. Figure 8 shows an illustration of such a scheme. This means that depending on the synchronization scheme followed there could be some decoupled sections that could be a full time-step behind the rest. Such a scheme necessitates the use of smaller timesteps to ensure that the decoupled sections don't diverge. This implies that in a meshed system being simulated on multiple cores the sequence of delays between different parts and their delay with respect to each other needs to be carefully designed to avoid divergence.

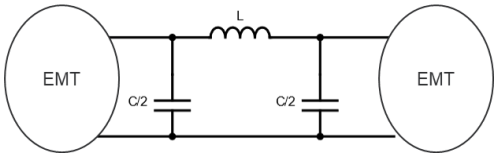

Figure 9: Stub line-based decoupling

And last, one of the classical approaches to decoupling networks involves leveraging propagation delays introduced by transmission lines. The inherent distributed inductance and capacitance (LC) components of long transmission lines ensure that a delay of one time-step or larger can be used to decouple sections of the network. While bulk grids often have several long lines that can

be used as convenient decoupling points, distribution lines usually are much shorter. Propagation delays associated with distribution networks are much smaller than a typical time-step used for real-time simulation. To overcome this issue, stub lines have been proposed as an alternative decoupling mechanism [22]. Stub lines are modeled as a shorter pi-line (Figure 9) that embeds a delay of exactly one simulation time-step (ts) by setting the LC components based on the relation ts = √ LC. While this approach serves to enable decoupling in distribution networks, it introduces LC components into the system that can alter reactive power flows across the network.

2.2 Custom Decoupling Scheme

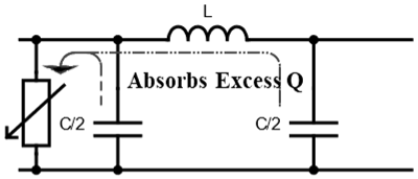

Figure 10: User Coded Decoupling Element with active compensation

The decoupling element emulates a stub line (LC) with a propagation delay of 1 timestep (in the case of this simulation, 50 µs). However, the C component of the stub line introduces erroneous reactive power into the system. The introduced reactive power influences the steady state power sharing patterns, as well as system dynamics during faults, topology changes, and other transients while deviating the solution from the no decoupling case. In this section, we propose a method to reduce this erroneous flow to allow decoupling without compromising accuracy. The decoupling approach used relies on making special considerations around this stub line model. Firstly, to ensure that the phase shift due to the inductance of the stub line is minimized, the 'L' component is kept significantly small in the proposed study. This implies that based on ts = √ LC for a given time-step the 'C' value will have to be large in order to introduce a single time-step delay for decoupling. This large capacitance introduces erroneous reactive power into the system. To remedy this excess reactive power, a compensation scheme is proposed around the decoupling elements. Figure 10 shows a representation of this approach. The objective of this compensation mechanism is to sink the erroneous reactive power at the decoupling element to ensure that flows across the system are unperturbed and closer to the ground truth power flow solution. Further, it is of importance to ensure that the introduced compensation mechanism doesn't exacerbate transients such as faults. To this end, the compensation scheme is designed to correct the erroneous reactive power precisely in steady state but introduce the correction slowly during large transients. Additional details about this scheme have been specified in [23].

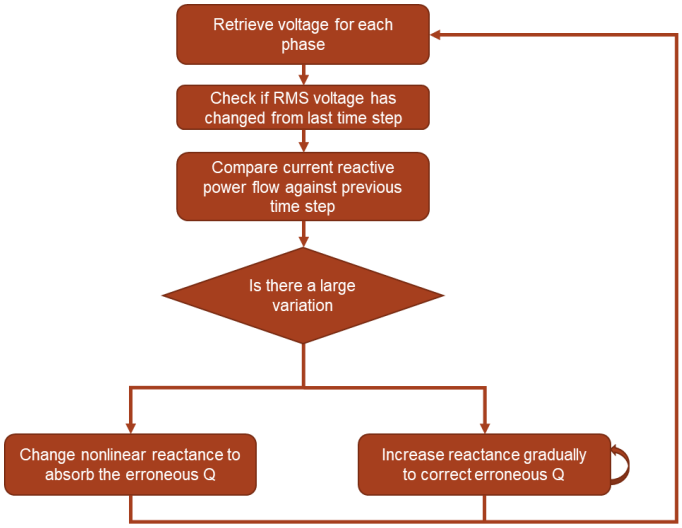

Figure 11: Decoupling Element Algorithm

Figure 11 represents a flowchart detailing the decoupling compensation technique. This approach ensures that the system stabilizes to a power flow solution closer to the ground truth without adding any excessive dynamics during fault scenarios. The compensation block is designed as a user coded model in OPAL-RT's HYPERSIM platform. Figure 11 represents a flowchart detailing the decoupling compensation technique. This user coded component developed as part of this work will serve as the building block for enabling multi-core simulations with a minimal loss of accuracy for our develop system models.

3.0 High-Fidelity Testbed Model

To assess vulnerability, security, resilience, and the impact of adverse conditions in microgrid based power systems, a high-fidelity model was built as part of this effort. The model consists of a physical layer that encompasses protective devices, RTU, RTAC, controllers coupled to a high-fidelity simulation model to embed the right level of fidelity and realism. It also comprises of a communication layer that can emulate data flows between control and hardware devices as closely as possible to derive valuable insights and metrics to measure attack vulnerability and allow rigorous experimentation.

3.1 Physical Layer

In order to study the behavior of microgrids with an increased penetration of DERs, we developed a model of the standard IEEE 123 node test feeder in HYPERSIM. While the topology of the feeder, the loads, and feeder parameters were based on the original specification as listed in [24], we added DERs at various locations by overlaying a logical three microgrid abstract structure based on the locations of the switches in the feeder. This logical structure allowed us to study grid-connected and islanded scenarios with each of the microgrids connected to each other and to the main substation feeder as needed.

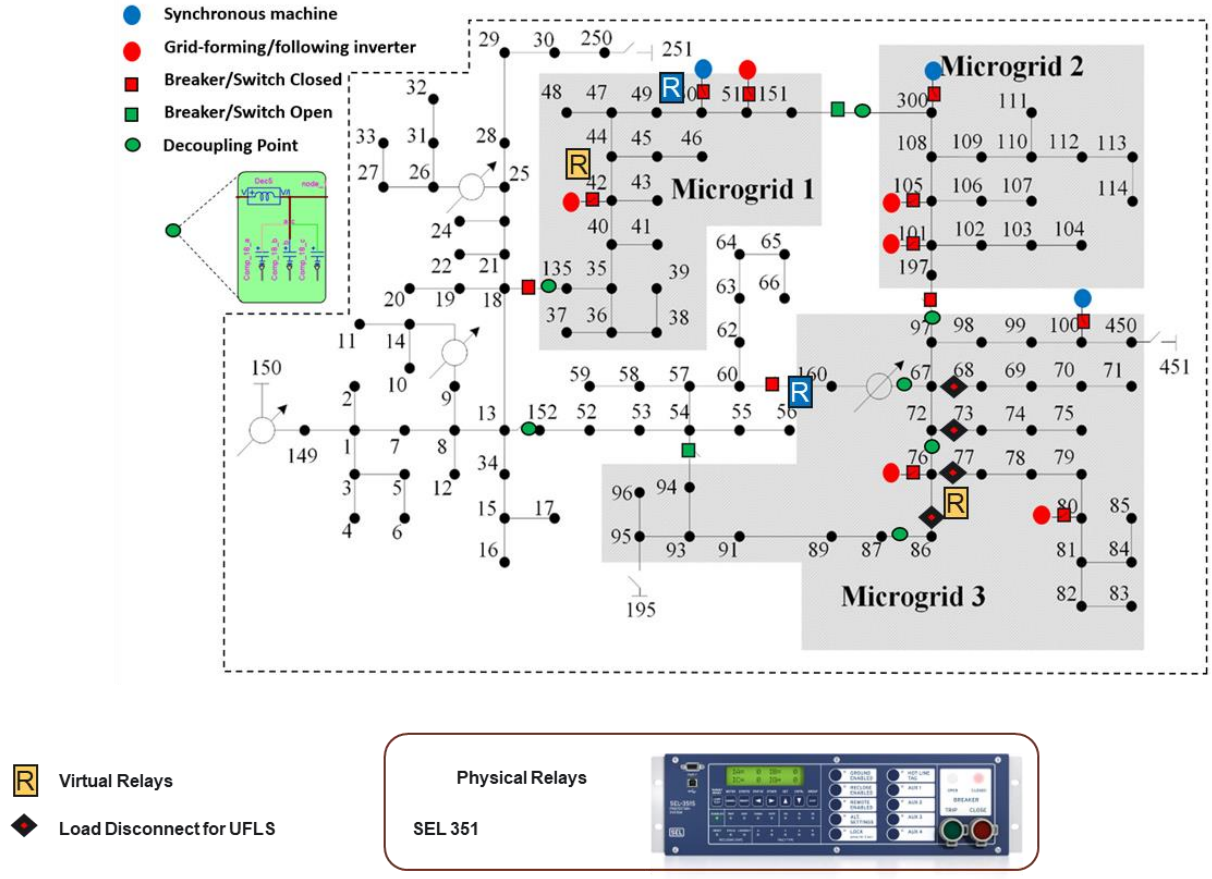

Figure 12: One-line diagram of the modified IEEE 123 node test feeder with decoupling points

Figure 12 shows a one-line diagram of our modified IEEE node test feeder model with the three microgrid logical structure. Each of the three microgrid boundaries are marked by the grey boxes,

while the remaining sections represent the distribution feeder that they are connected to. In our base case, all these microgrids are connected to the main feeder and effectively the voltage source through sectionalizing switches. All of these switches could be reconfigured dynamically to study specific tests/scenarios.

Each microgrid has three DERs to support islanded operation. There are two inverters (grid-following and grid-forming) and one diesel generator in each of the microgrids as shown in Figure 2. Blue dots show the position of the diesel generators, and the red dots show the positions of grid-forming and grid-following inverters. Red boxes show the positions of breakers/sectionalizing switches in the model.

3.1.1 Controls

Each synchronous machine has an excitation system and a speed governor modeled. Specifically, we have a standard AC1A exciter and DEGOV1 governor modeled, however this could be modified to other types if needed. We have active power/frequency droop setup on the generator and the settings for exciters and governors can be adjusted dynamically. Figure 13 shows a depiction of the developed synchronous machine models. For each grid-following and grid-forming inverter in the microgrids, we assume that they are Photovoltaic (PV) interfaced with a switching frequency of 10 kHz. We have modeled generic current and voltage control loops with the ability to adjust active power/frequency (P/f) and reactive power/frequency (Q/V) droops, active/reactive power setpoints, and voltage setpoints. For the PV modules, we can also adjust the irradiance levels, if needed. These inverter models were developed by an ancillary effort [25], [26] within the RD2C initiative and integrated by through this work into the testbed.

3.1.2 Protection

There are a combination of physical SEL [27] and virtual protection relays in our testbed that are integrated into our model. The physical relays are connected through low-voltage analog and digital interfacing while the virtual relays are just protective functions such as overcurrent, over/under-frequency elements modeled directly on the real-time simulator. Depending on the use cases studied, we map both physical and virtual relays to specific locations on the microgrid appropriately. Figure 12 shows the physical relays placed at certain candidate locations for some use cases.

3.1.3 Real-time Decoupling

As stated earlier, simulating large systems at high fidelities with all the associated controls, protection elements at small time-steps is challenging. In our case, for the specific simulator hardware that we are utilizing, the aforementioned model without any decoupling had a total computational time of about 150 µs. This meant that we could not run the model in real-time with a typical EMT time-step of 50 µs. In order to bring the overall computation times lower and to maintain a time-step of 50µs, we added several decoupling elements at seven locations as shown in Figure 2 by the green dots. These decoupling elements allow the computational burden to be divided up on multiple processors to allow strict real-time execution. In order to compensate for the errors in reactive powers due to the decoupling elements, which are essentially a small line segments, we also included our shunt reactive power compensation components that would adaptively adjust the reactive power compensation to provide based on the system voltages.

3.1.4 Custom Libraries

In the process of translating this model from GridLAB-D to HYPERSIM a lack of counterpart components was observed. To bridge the gap, several models were developed and added into a custom library. The following models were developed in addition to the decoupling block summarized above:

- Single-phase constant power load
- Single-phase delta connected constant power load
- Phase breakouts – Owing to the prevalence of balanced three phase models typically observed, breakouts for single-phase and two-phase components had to be developed to model the three-phase unbalanced network in Figure 12.

3.2 Communication/Control Layer

The real-time model also includes 4 virtual remote terminal units to stream telemetry corresponding to various voltages and currents across the three microgrids and the main feeder through the Distributed Network Protocol - version 3 (DNP3) protocol to an Open Platform Communications (OPC) server, which acts as a data aggregator at a control center. Further, it also includes virtual device controllers for the inverters so that they can receive secondary control commands as well as send measurements from/to external sources via the Modbus protocol. Each of the microgrid thus has it's own emulated network and control structure. The DNP3 sensors send voltages and currents from specific locations to the OPC server. Figure 13 shows the sensor locations. The realized network architecture and its integration with the model described in the previous section is shown in Figure 14.

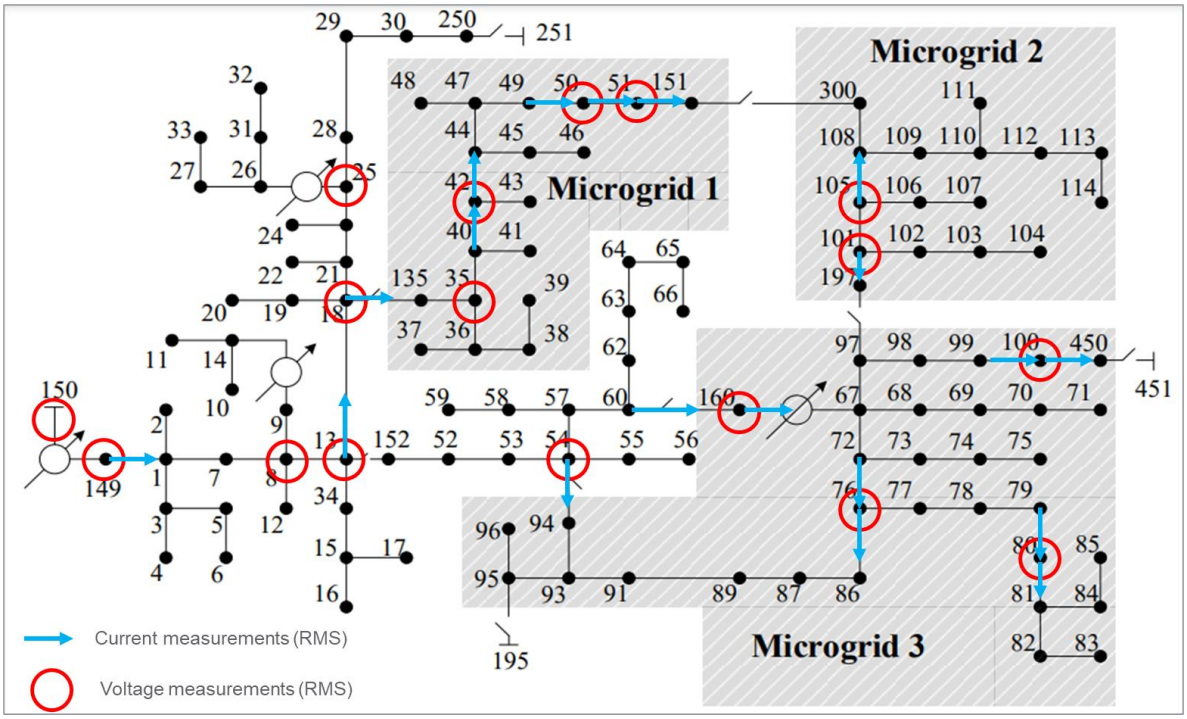

Figure 13: DNP3 Sensor locations

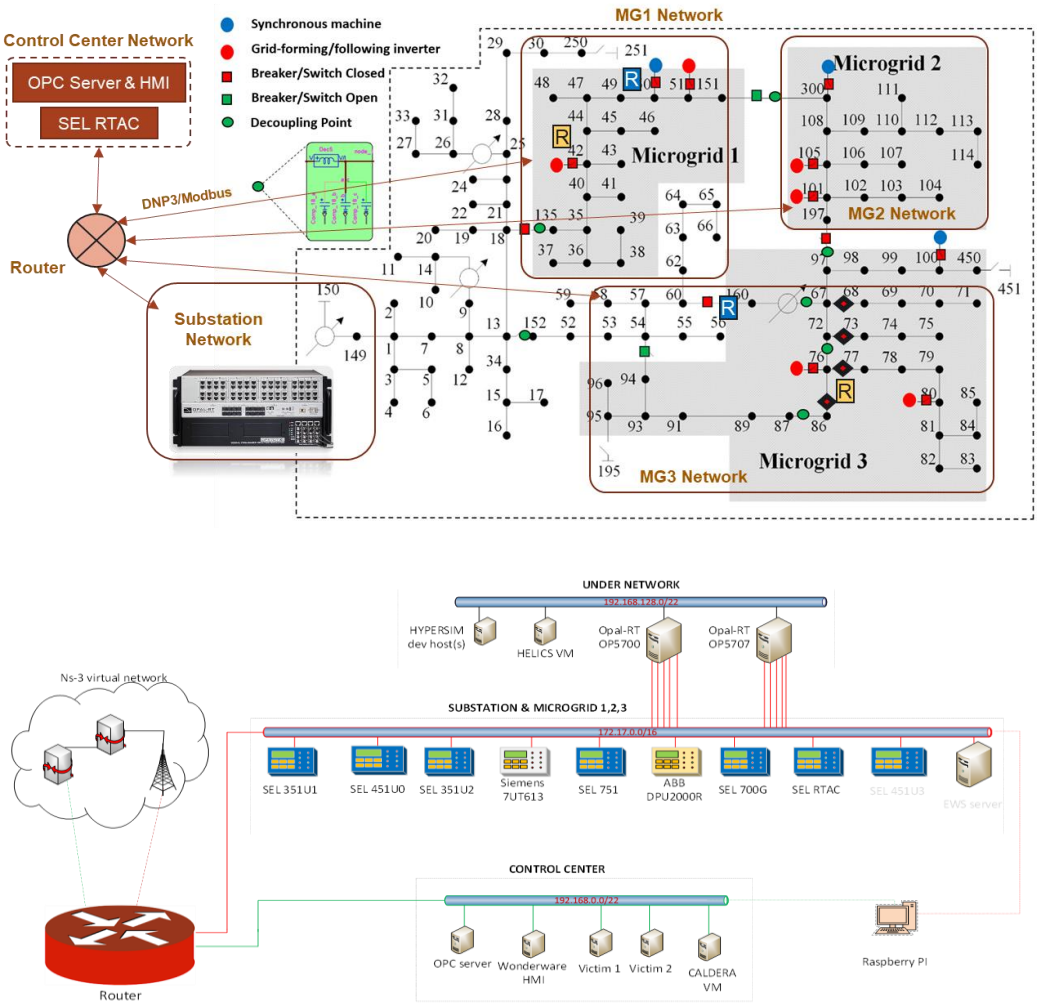

Figure 14: Network Layer and Integrated cyber-physical testbed

3.3 Model Validation and Benchmarking

To ensure that the translated model and the developed components are accurate, baseline studies were conducted to ensure that the flows across the system, voltages and currents matched those seen in the original template GridLAB-D model. The process involved 2 key aspects – validating model performance under steady state and dynamic conditions.

3.3.1 Steady-state Model Validation

The first being a static validation. This process was centered around steady state conditions. The voltages across a steady state operating condition were captured in the GridLAB-D model as well as the developed testbed 123 node network. The deviation between the two models was measured in the form of voltage differences seen at all nodes across the network. Since, the feeder is an unbalanced network, the individual phase voltages were compiled, and the average deviation was captured on a per-phase basis. Figure 15 shows a bar chart summarizing the

deviation in voltages seen. The deviation observed was small and is expected when comparing results from two different solvers computing power flows in different domains (EMT and Phasor).

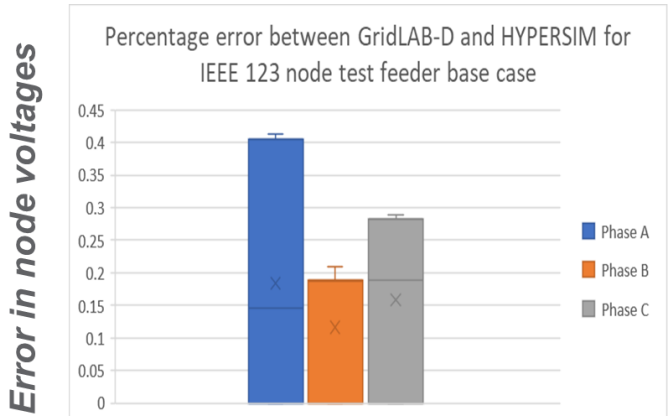

Figure 15: Node voltage deviation from original GridLAB-D template model under steady state conditions

3.3.2 Validation of Model Performance under Dynamic Conditions

In this section, we will present the results from a few use cases that were conducted to show the effectiveness of the proposed decoupling solution under steady-state and dynamic conditions. Specifically, we intend to compare three different cases to evaluate the performance. They are as follows:

• Case 1 - Base case without any model decoupling

• Case 2 - With decoupling elements and no compensation

• Case 3 - With decoupling elements and compensation

3.3.2.1 Steady-state:

Here, we compare the instantaneous waveforms for power from all the sources and the current across the locations of decoupling elements in the model for three different cases. Figure 16 illustrates that the source power for all the cases are slightly different, with a lower peak value of source power for the case consisting of decoupling element without any compensation. This shows that the power draw from the feeder head and the power sharing pattern is slightly altered by introducing decoupling elements without compensating for the erroneous reactive power. Similarly, the instantaneous power for generators, grid-following and grid-forming inverters are slightly different as seen in Figure 17, with minor deviations in peak value for case consisting of decoupling element without any compensation in generators and slight phasor deviation in power for grid-following inverters for case consisting of both decoupling and compensation element.

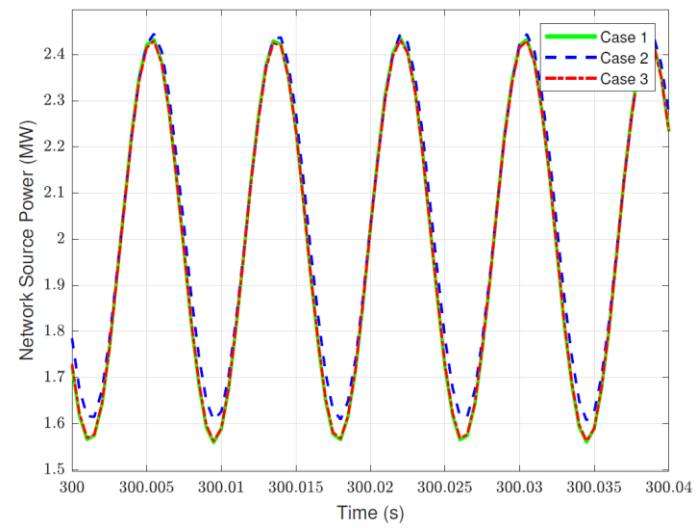

Figure 16: Comparison of source power output for the three cases proposed

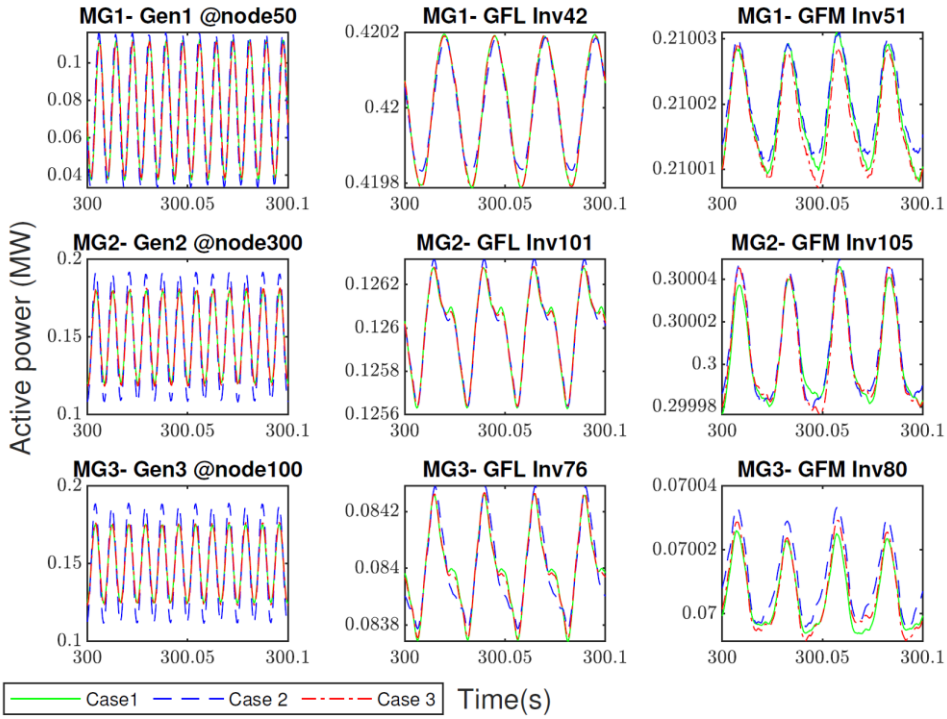

Figure 17: Comparison of active power outputs for generators and inverters for all cases

Figure 18 shows the deviation of the Root Mean Square (RMS) values of the current across the decoupling elements with respect to the base case. The cases with models consisting of deviation in current with respect to the base model has been minimized using the compensation approach. This shows that the compensation scheme allows effective decoupling to enable multi-core simulations without compromising the accuracy significantly. Further, the voltage

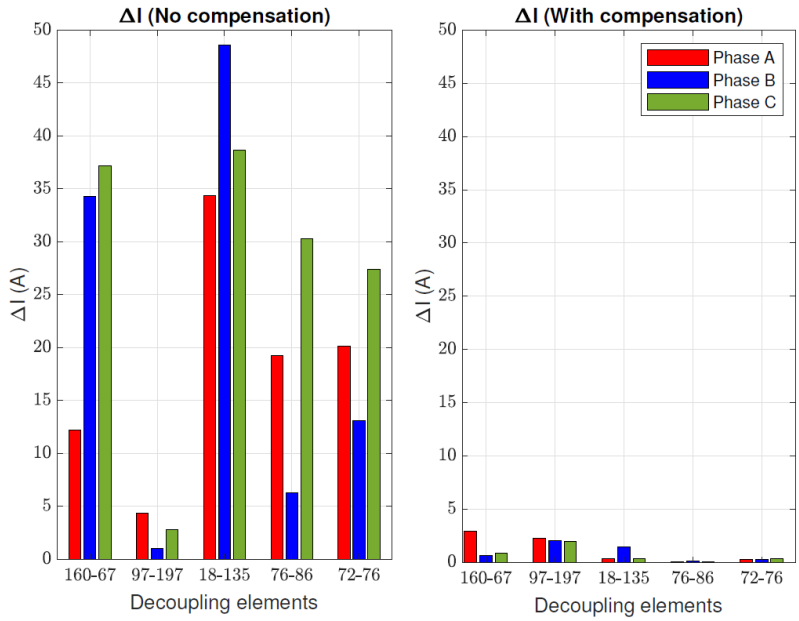

Figure 18: Comparison of current across the decoupling elements.

deviation for all the nodes with respect to the base case is calculated and the statistics for the deviations are shown in the box-plot in Figure 19. It can be seen that compensation for the decoupling elements reduces the voltage deviation in the nodes with respect to the base case. This proves that the errors in the node voltage are minimized, and the base case is replicated correctly with the decoupling approach with the added compensation. Thus, it can be noted that the combination of decoupling elements and compensation assists in replicating the steady-state operation of the base case model with minimal errors.

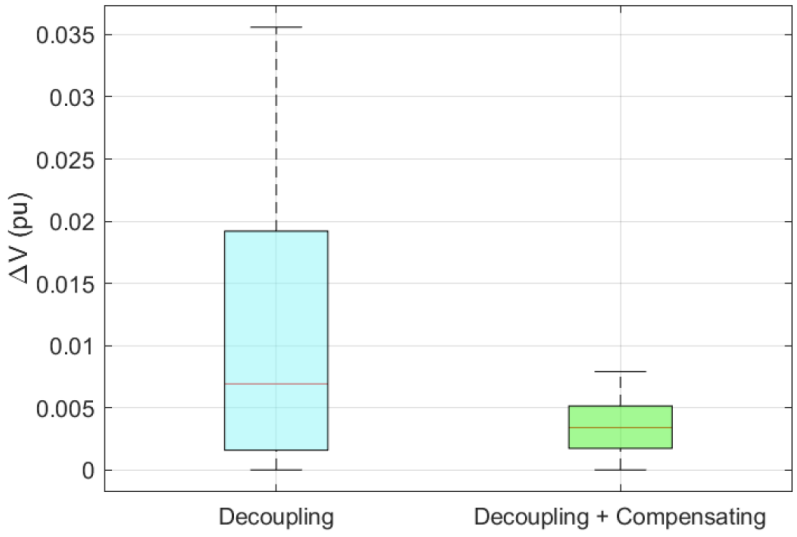

Figure 19: Box plots of voltage deviation for all nodes relative to the base case

3.3.2.2 Dynamic Conditions

In order to compare the performance and accuracy of the decoupling approaches a scenario is simulated where a fault occurs at the terminals of an inverter at node 80. The fault is cleared rapidly by isolating the inverter and reconnecting it out of sync. Figure 20(a) shows the event and the active power output of the associated inverter. To examine the loss in accuracy, the current across the decoupling element between nodes 13 and 152 is plotted in 3 cases in Figure 20(b). Case 1 signifies the base case or the ground truth current. Cases 2 and 3 show the current across the link when using a decoupling element without compensation and the modified decoupling element with the compensation scheme proposed earlier respectively.

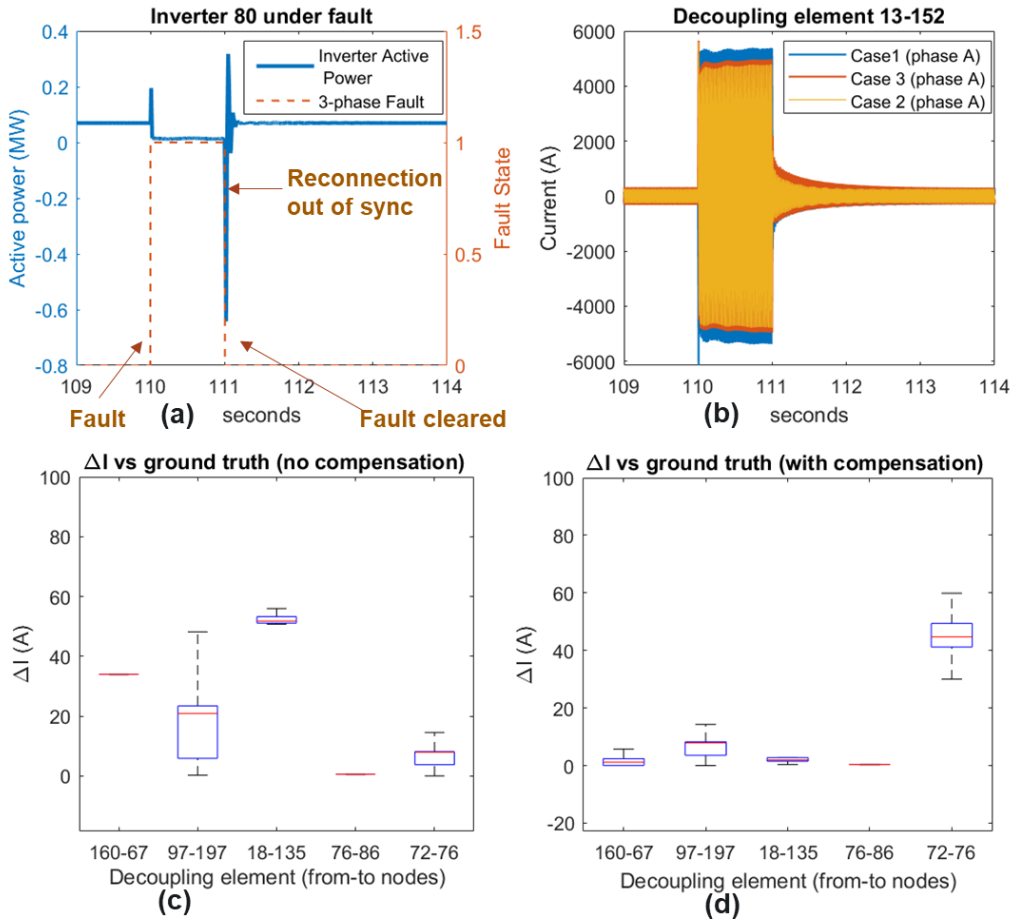

Figure 20: Comparison of system parameters under a three-phase fault

The results show that the compensation scheme reduces the deviation from the ground truth while still enabling the use of multi-core computations. It is seen that the compensation scheme does not exacerbate the transient or compromise the accuracy of the transient response. Moreover, it serves to correct the effect of excess reactive power flow caused by the stub line. Figure 20(c) shows the average current difference across the other decoupling elements when compared with the base case. It is seen that on an average across all three phases the deviation from ground truth is quite significant.

Figure 20(d) shows the average current difference across the other decoupling elements when using a compensation scheme. It is observed that the deviation in current and thereby flows across the system in relation to the ground truth are minimized using this compensation scheme. While a difference is observed in this scenario, the full extent of the deviation in relation to the electrical distance of a given event from decoupling elements with compensation need to be investigated in future studies. Our studies show that the proposed compensation approach adapts the level of compensation based on transients and minimizes the errors introduced overall while compared to no compensation approach.

4.0 Use-Case Generation and Scenario Orchestration

The developed testbed model allows validation and prototyping of advanced controls with protection devices in the loop along with a realistic communication framework to assess vulnerability and information flows. This further allows creation of rich datasets that can analyze specific dynamics, adverse conditions, and attack impacts. To create these datasets, it is vital to create a pipeline that allows user input in the form of specific events that need to be triggered as the model is simulated. To allow this an orchestration pipeline was built using the HYPERSIM API functionality. This allows specific events to be triggered at specific timestamps (15 seconds intervals). The orchestration pipeline ingests a user generated csv specifying load/parameter changes and orchestrates a 600 second simulation while coordinating these events. Figure 21 shows a flowchart detailing the orchestration process and shows a snapshot of the log detailing simulation changes. This allows multiple use cases and scenarios to be created and datasets to be generated. Using this tool rigorous analysis of novel controls or system modes can be conducted. The orchestration script is written in Python and communicated directly with the HYPERSIM user interface.

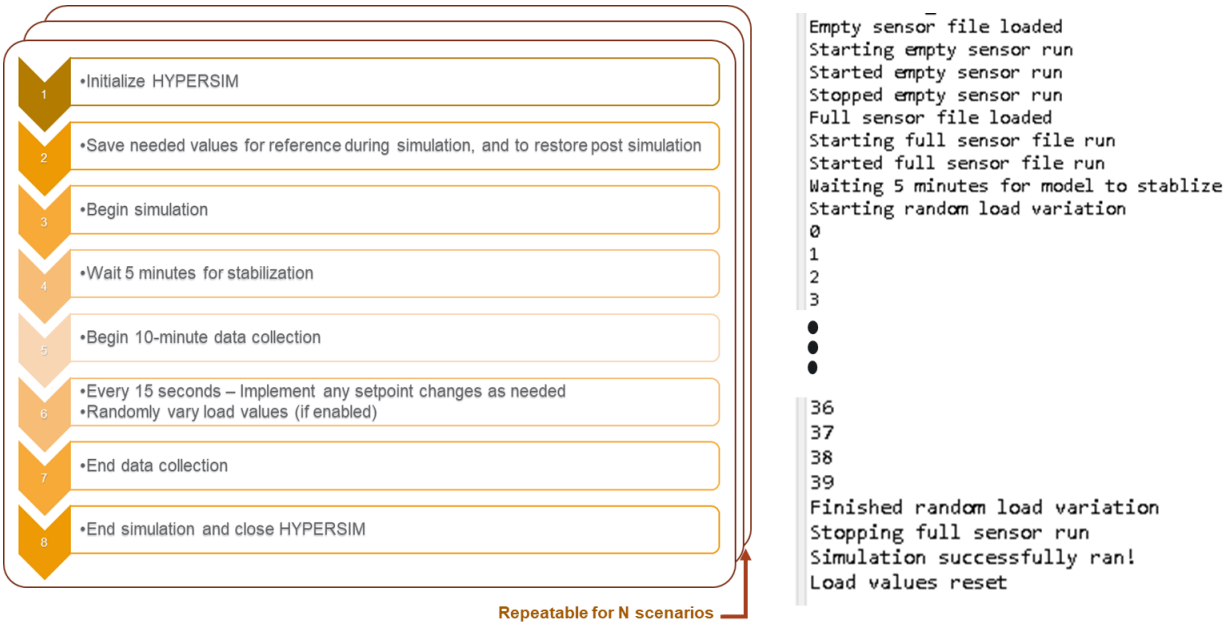

Figure 21: Automation and Orchestration using the HYPERSIM API

By utilizing this pipeline, a variety of datasets can be captured. The captured datasets contain data both from the physical layer as well as the cyber layer. The datasets capturing physical layer quantities (voltages, current, frequencies and specific inputs and outputs) are found in a proprietary OPAL-RT format (‘.oprec’ files). Similarly, the network data is captured in the form of packet capture files (‘.pcap’). A secondary orchestration script is developed to encapsulate the one listed in Figure 21 that can trigger network simulation through the aforementioned pipeline, start network data capture, compile the collected physical and cyber layer data, convert it into non-proprietary format (‘.csv’ files) and generate diagnostics to ensure data integrity. This secondary orchestration pipeline also enables orchestrated attacks to be injected on to the network layer in addition to the events on the power network orchestrated in Figure 21. Figure 22 provides a process overview of the secondary pipeline. The attacks are orchestrated using the MITRE Caldera framework [28].

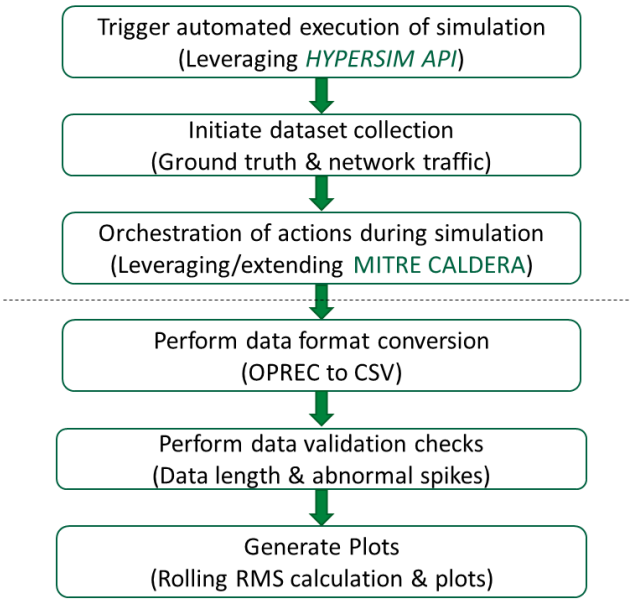

Figure 22: Secondary Orchestration Framework

Utilizing a combination of these two pipelines it is possible to orchestrate multiple cyber-physical events and analyze risk, identify attack surfaces, create adverse and off-nominal conditions and test remediation actions. The next section details the specific attributes of the generated datasets.

5.0 Dataset Attributes

The orchestration pipelines summarized above allow repeated execution to create a variety of scenario sand their associated datasets. Specific attributes of the physical and cyber layer datasets will be detailed in this section.

5.1 Physical Layer Datasets

Each scenario that is orchestrated produces a dataset containing the following quantities:

- All node voltages from the 123-node feeder
- All load real and reactive power consumption
- Source node voltages
- All generator set points, real and reactive power output and frequency at terminal nodes
- All inverter set points, real and reactive power outputs and terminal frequency

The simulation model operates with a timestep of 50 µs. However, the data is captured with a decimation factor of 10. This implies that the resolution of the captured data for all the above quantities is 500 µs. This was done to avoid over inundation of datapoints since the captured resolution is sufficient for most studies. Figure 23 shows a snapshot of the captured 500 µs data for a template scenario.

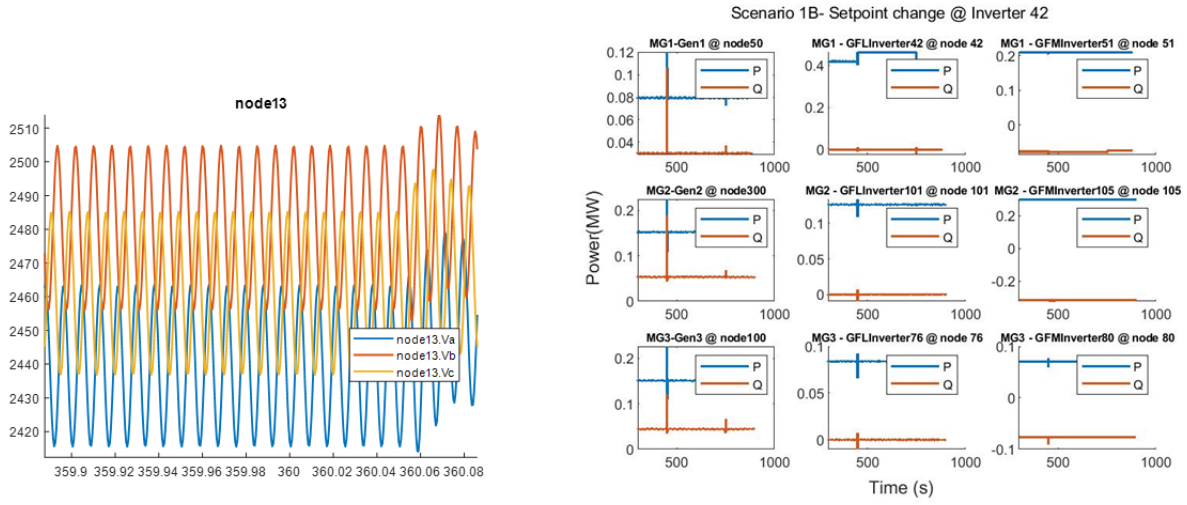

Figure 23: Sample waveforms/diagnostic plots detailing the nature of the datasets

The data is collected and split into 5 different files. Three of these contain parameters listed above for the three microgrids in the network, one of them contains data about the rest of the feeder while the last one contains data that was exchanged over the network with controllers or the OPC server.

5.2 Network Layer Datasets

As mentioned in the previous section, the accompanying data flows including quantities exchanged with protective relays or controller as well as the network data exchanged in the form of Modbus setpoints issues by the OPC server or the DNP3 measurements sent from the network are vital to assessing the impact of specific protective functions, assessing attack vulnerability and assessing the impact of specific data integrity and command injection-based attacks. To ensure that the datasets capture these information flows, the orchestration pipeline specified earlier captures all the dataflows in a packet capture file for a given scenario. Data flowing to and from integrated hardware-in-the-loo (HIL) devices (relays, amplifiers) can also be captured here. Figure 24 shows a sample DNP3 packet captured during a template scenario.

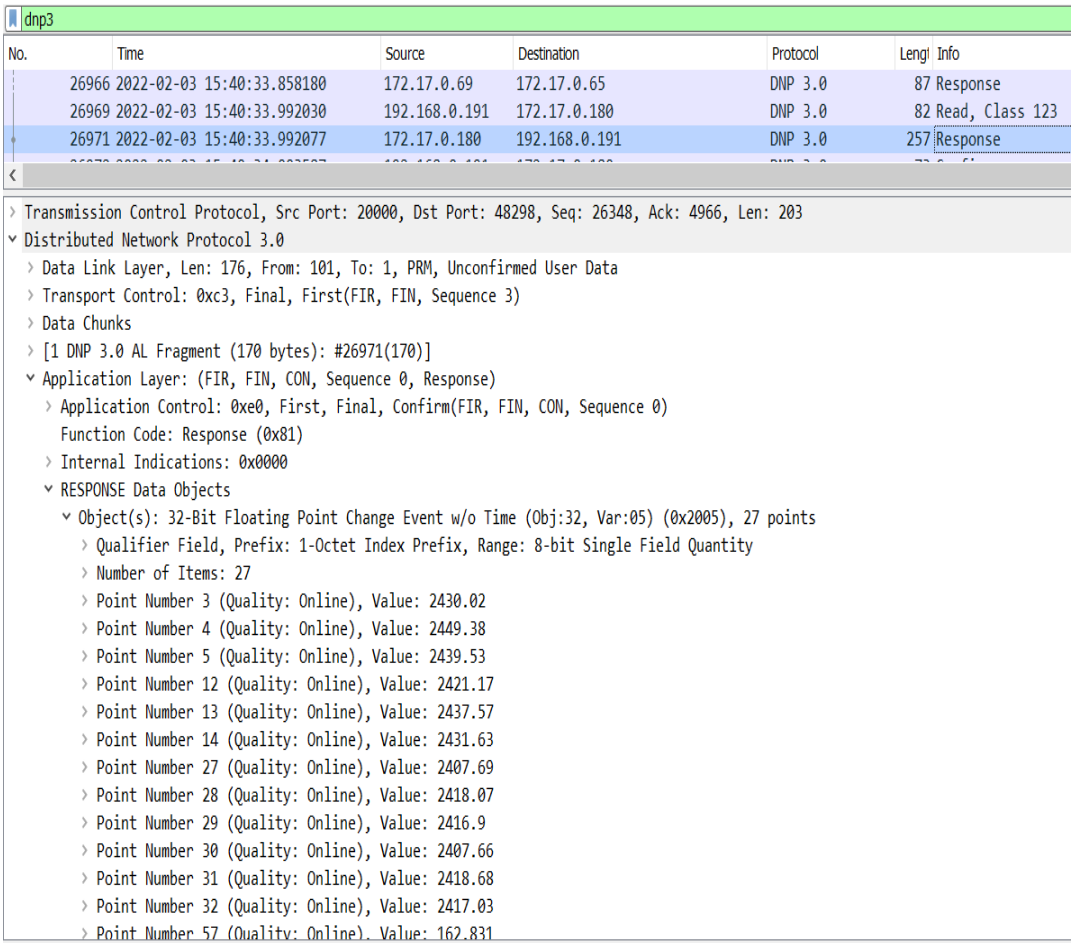

Figure 24: Sample DNP3 packet from the captured dataset

By correlating the information between the physical and network layer datasets, a complete picture of all system interactions in the form of grid and control dynamics can be derived to perform meaningful analysis. The next section details a range of datasets that were generated to aid analysis centered around control, resilience and attack vulnerability. All generated datasets have been stored on an internal PNNL repository to allow research teams to utilize them effectively.

6.0 Experiments and Datasets

A variety of datasets were generated as part of this work to reflect numerous operating conditions across the 123-node test feeder model. These conditions were simulated to reflect the complexity of operating microgrids in grid-connected, islanded and networked modes. Transients associated with microgrid reconnection were analyzed from an operational standpoint. A second set of experiments involved generating datasets centered around attack scenarios. These scenarios were focused on capturing the grid dynamics and the associated effects on grid stability when an attacker was able to manipulate system settings, inject attacks and trigger specific grid conditions that would result in sub-optimal operation. The developed scenarios can be classified as shown in Figure 25. Details about the generated experiments are provided in the next few subsections. The generated datasets are stored in a repository on the Research computing resources and are available to all projects within the initiative. The team is currently exploring options to make the datasets widely available on DataHub [29]. Each of these scenarios have been designed in consultation with subject matter experts exploring numerous uses for testbed data and have been utilized for testing and validation. Diagnostic plots describing the scenarios may be found in the repository. Plots for a couple of interesting cases are presented here in this report.

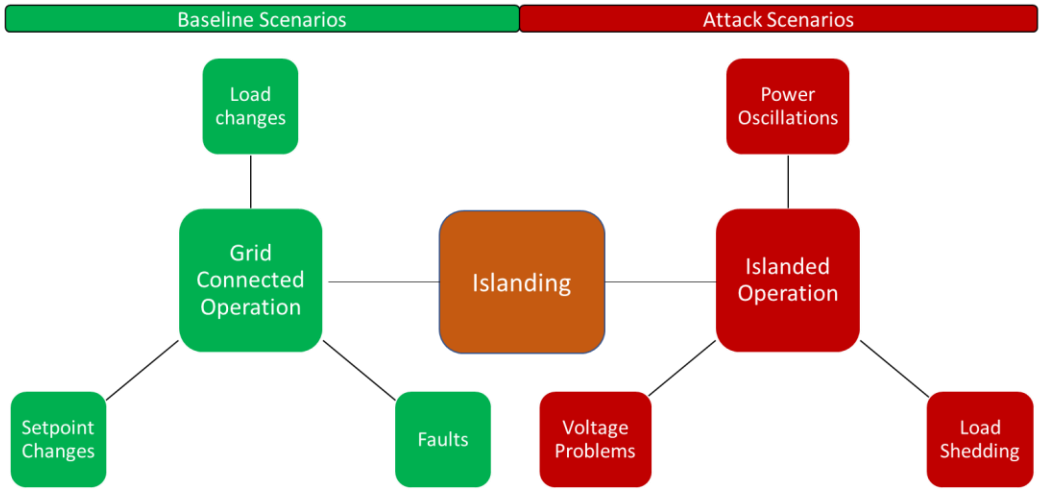

Figure 25: Use cases for experimentation

6.1 Scenario 1A and 1B

This scenario is designed to analyze the sensitivity of system flows to step changes within the 123-node feeder while in grid-connected mode. Scenario 1A deals with creating a targeted step change in a single load in the system. This involves increasing the load at a specific timestep and decreasing it later in the capture window to understand changes in voltage profiles, current flows and power sharing patterns between the inverters, generators and the substation node. 7 locations for load step changes were chosen leading to 7 high-fidelity datasets for scenario 1A.

Similarly, scenario 1B is designed to issue step changes to the power references for the 6 inverters in the system. As part of this scenario, the active power set points of the inverters were increased and decreased to observe the change in system states. Both of these scenarios haven been used by projects within the initiative to understand the sensitivity of the system to step changes and have aided in creating physics informed mathematical models of the system in

numerous control algorithms. Figure 26 shows the locations of the loads and inverters chosen for scenario 1A/1B.

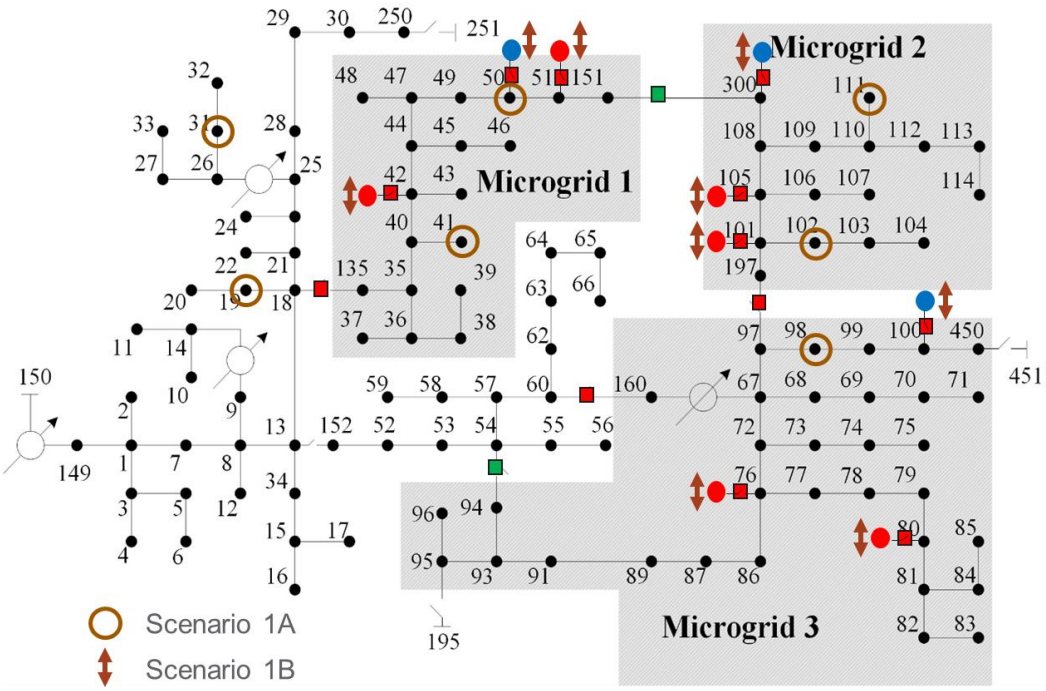

Figure 26: Scenario 1A/1B locations

6.2 Scenario 2A and 2B

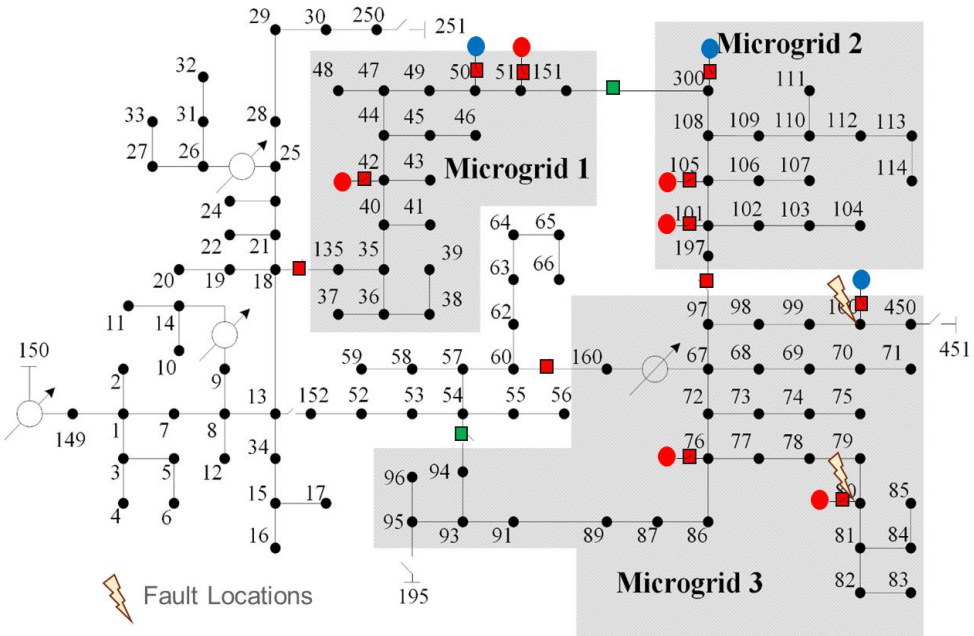

Figure 27: Fault locations for scenario 2A/2B

Scenario 2 is centered around analyzing the system's response to a 3-phase line-to-ground fault in grid-connected mode. To do this a timed fault is introduced using the aforementioned

orchestration pipeline near a source. The fault results in a nearby overcurrent relay tripping and disconnecting the generating source. The fault is subsequently cleared and the source is reconnected to the system. The scenario serves to show the effect of a fault as well as describes the reconnection transients typically seen in the system. Figure 27 shows the locations of the fault points and the two sources affected by it. To capture the reconnection transients produced by different types of sources, the fault locations were placed at a generator (node 100) and a grid-forming inverter (inverter 80) for scenarios 2A and 2B respectively.

6.3 Scenario 3A,3B and 3C

Scenario 3 deals with creating a command injection attack on the feeder to create unintentional islanding conditions. Figure 28 details the layout of the system and the location of specific physical SEL relays in the system. These relays are part of the system using n HIL approach and are signified by the blue boxes. A under-frequency load-shedding scheme (UFLS) [30]is put in place on four laterals in microgrid 3 seen as black dots with a red rhombus in the figure. This scheme is implemented by using frequency meters and virtual relays (relay blocks within HYPERSIM). The UFLS scheme sheds load depending on the frequency transient in question.

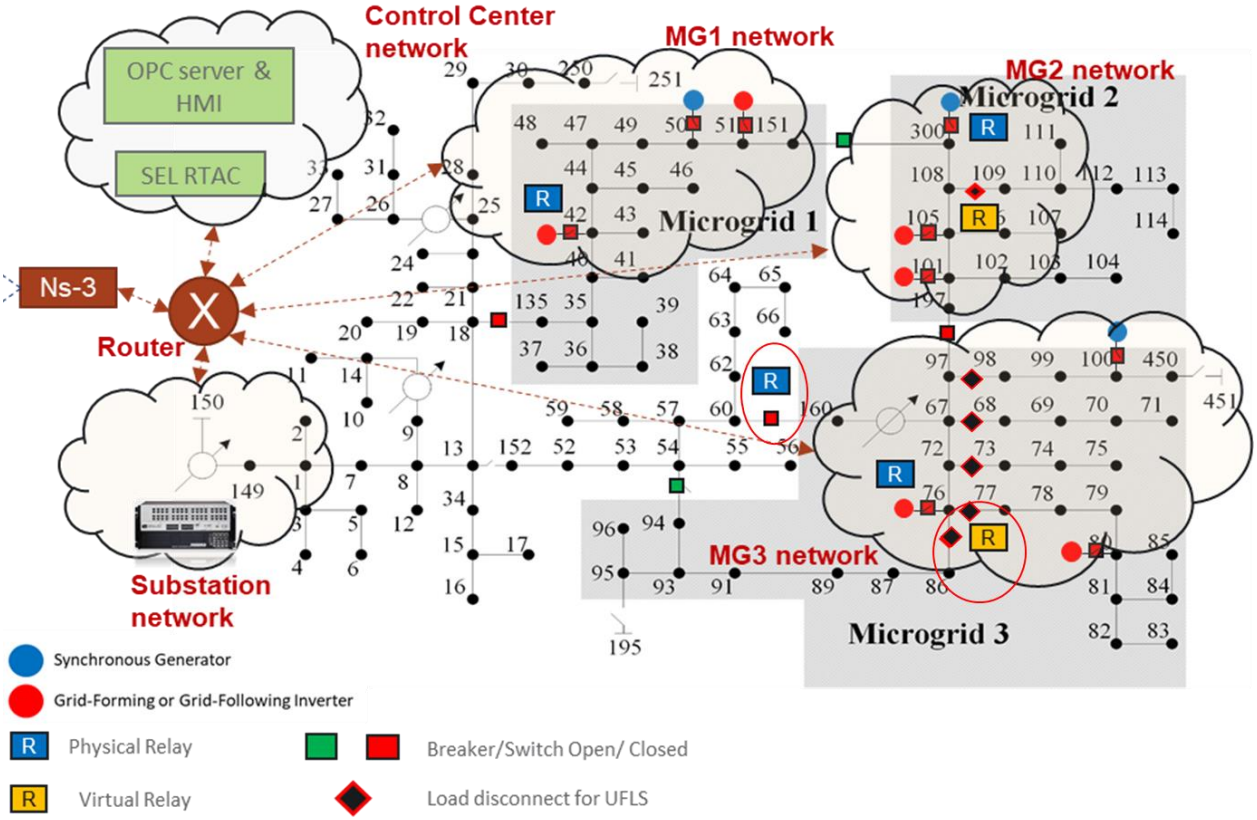

Figure 28: System setup for command injection scenario

Scenario 3A involves a command injection attack that manipulates a remote bit on the SEL relay highlighted in the red circle. This causes the relay to trip erroneously and island microgrid 2 and 3 together. Owing to the unintentional nature of the islanding operation, large transients are observed. These large frequency transients further cause the UFLS scheme to trip some of the laterals resulting in unintentional load shedding. The scenario serves to show the effect of a

malicious attack on a system with just a single point of control and operation. The large transients observed as a result of this event are shown in Figure 29.

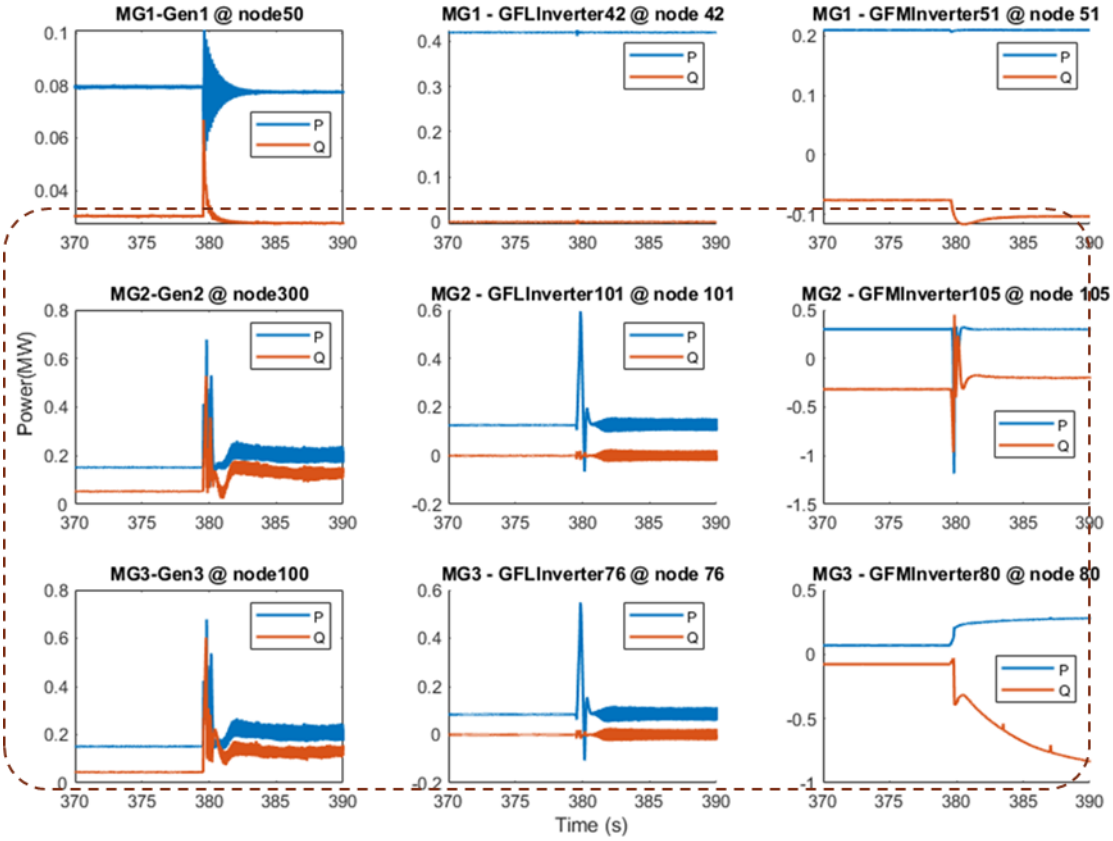

Figure 29: Command injection creating forced islanding.

Scenarios 3B then attempts to issue a dispatch change and shows the reduced transients from such an event reducing the response of the UFLS scheme. Scenario 3C introduces 2 points of attack where the settings on the UFLS relays are also manipulated by the attacker to combine the islanding transients with a failure of the UFLS scheme. The diagnostic plots for these can be found on the shared repository for the same. Scenario 3 thereby introduces the effect of a command injection attack with different levels of control exerted by the attacker on the system.

6.4 Scenario 4A and 4B

Scenario 4 begins with the system in islanded mode. Microgrid 1 is islanded and microgrids 2 and 3 are islanded as a group. As opposed to scenario 3 where the attacker was able to gain access to protective devices, this scenario explores the effect of a man-in-the-middle (MITM) attack. Here an attacker is able to gain control over the secondary control structure embedded in the OPC server and manipulated set points for specific generating sources. As a first step, the attacker is able to change droop characteristics on certain grid-following inverters in the system. In this instance, the attacker is able to manipulate the Q-V droop and the reactive power setpoint to effectively make the inverter at node 42 absorb large amounts of reactive power causing a voltage sag in the islanded microgrid 1. This attack is captured in scenario 4A.

Scenario 4B involves the attacker also gaining access to the active power reference for inverter 42. The attacker then varies this setpoint rapidly to create large power oscillations on the islanded system. While typical protection functions within the microgrid would certainly trip under these conditions, the scenario is aimed to show how this attack coupled with the attacker gaining control over protective device settings can cause sustained oscillations in islanded microgrids. Figure 30 shows a system schematic detailing the nature of the attack. Figure 31 shows the power outputs and the observed terminal frequency as well as the inverter's internal frequency during this event.

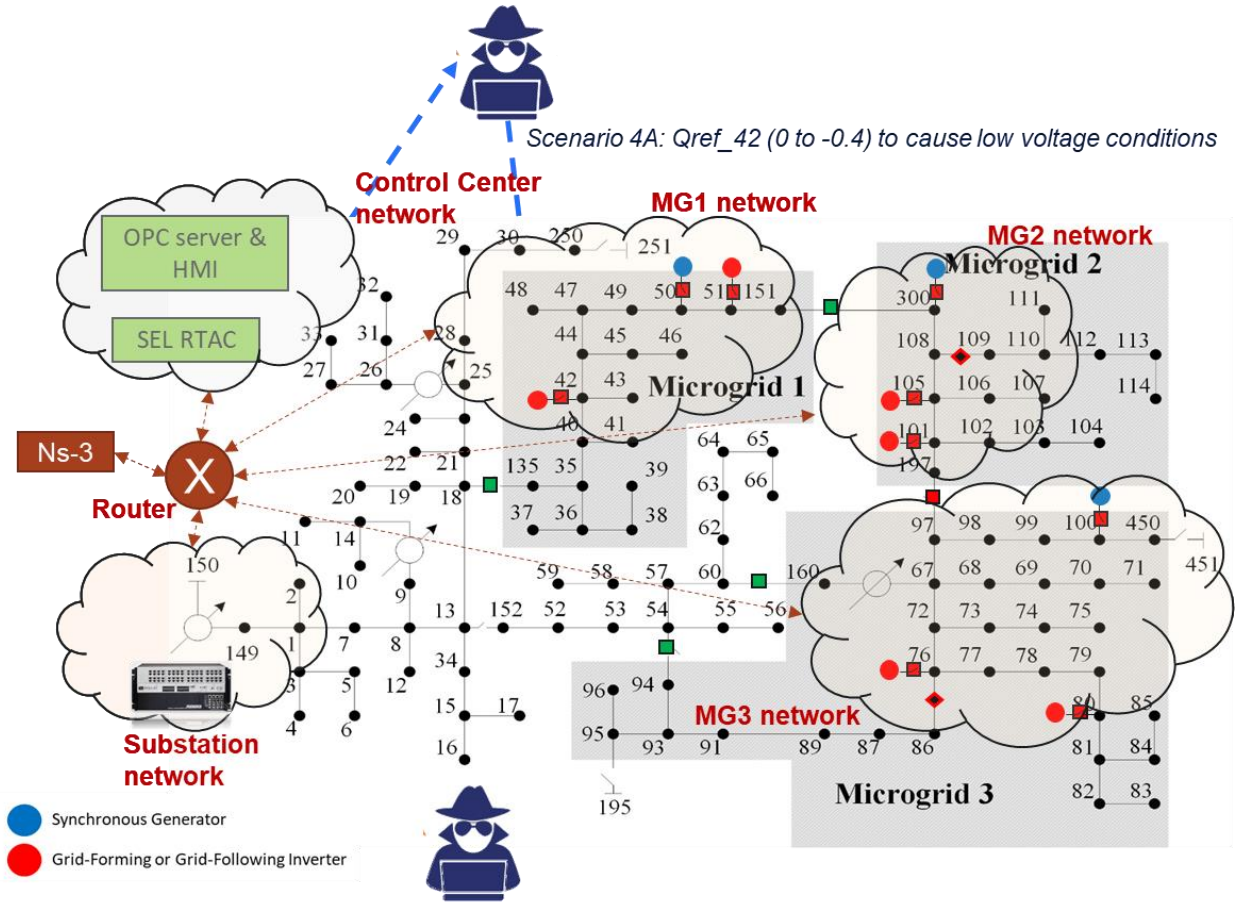

Figure 30: Scenario 4A and 4B attack description

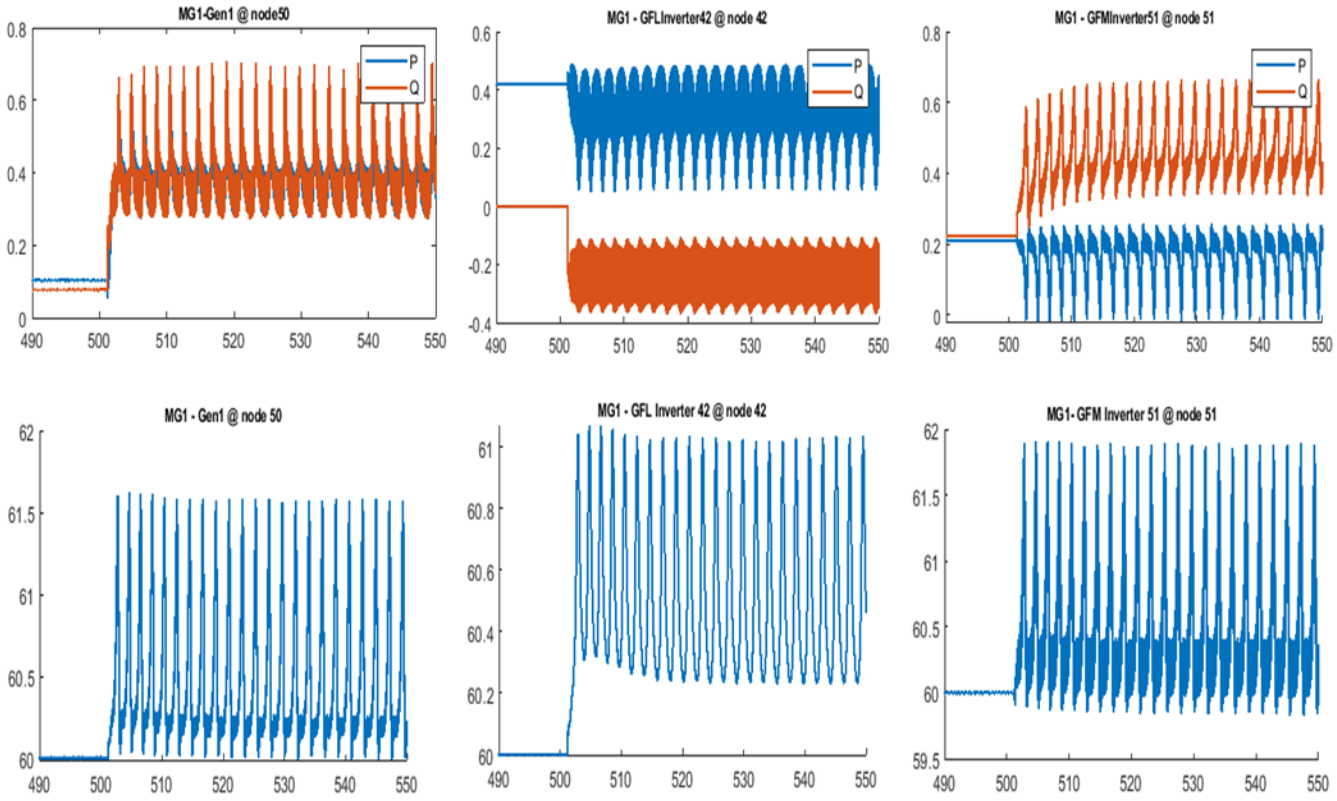

Figure 31: Power outputs of the three generating sources in microgrid 1 in MW (top). Synchronous machine speed during attack (bottom left). Internal frequency in the control loops of inverter 42 and 51 during attack (bottom right)

6.5 Scenario 5

Scenario 5 begins with the system in islanded mode. Microgrid 1 is islanded and microgrids 2 and 3 are islanded as a group. This scenario centers around an attack model centered around disconnecting a generator and reconnecting it out-of-step. The relay connecting generator at node 50 is manipulated through command injection to trip the generator and reconnect it out of sync. While, this scenario damages the shaft of the generator, this scenario centers around assessing the dynamics introduced on the rest of the microgrid. Figure 31 shows the location of the relay and the generator being attacked. The location is highlighted in a red circle on the figure.

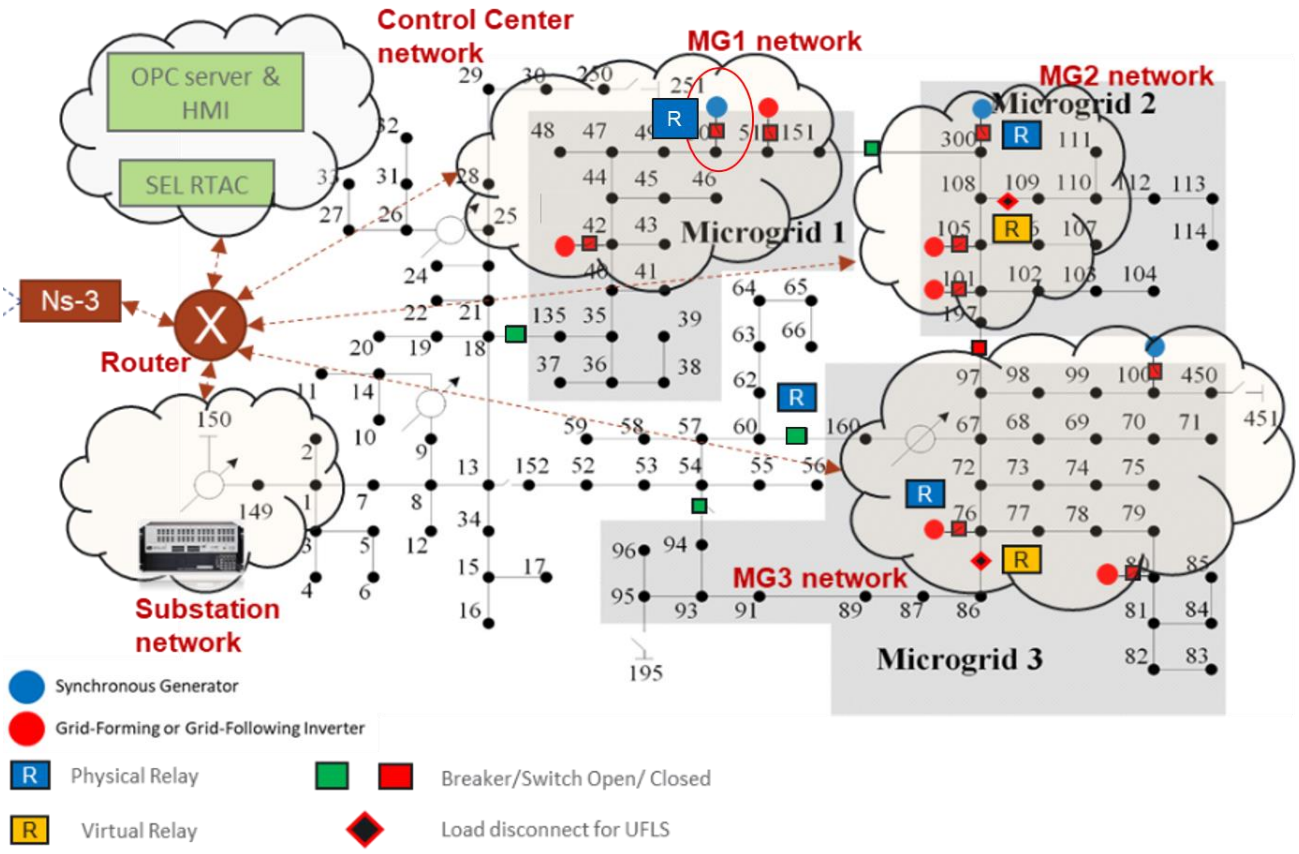

Figure 32: Scenario 5 – Command injection to assess vulnerability in a microgrid environment

6.6 Scenario 6

Lastly, scenario 6 deals with a complete islanding scenario. The system is initialized in a grid-connected mode. A command injection attack like scenario 3 is carried out to island microgrid 2 and 3 as an island and microgrid 1 as an island. Further, microgrid 2 and 3 are separated from each other using virtual relays to operate 3 independent microgrids. This scenario is of interest due to the specific generation-demand balance issues specific to each microgrid. The conditions are specified below:

- Microgrid 1 – Has an adequate supply-demand ratio and survives the transition.
- Microgrid 2 – Has a generation surplus and causes over frequency conditions that cause the diesel generator at node 300 to trip.
- Microgrid 3 – Has a deficit in generation capacity and goes into under frequency conditions causing the UFLS scheme to trip load

It is important to note that when microgrid 2 and 3 were operating as an island in the previous scenarios, the surplus generation in microgrid 2 was able to cover the deficit in microgrid 3. The relay being subjected to command injection and the sections of microgrid 2 and 3 being tripped are shown in Figure 33.

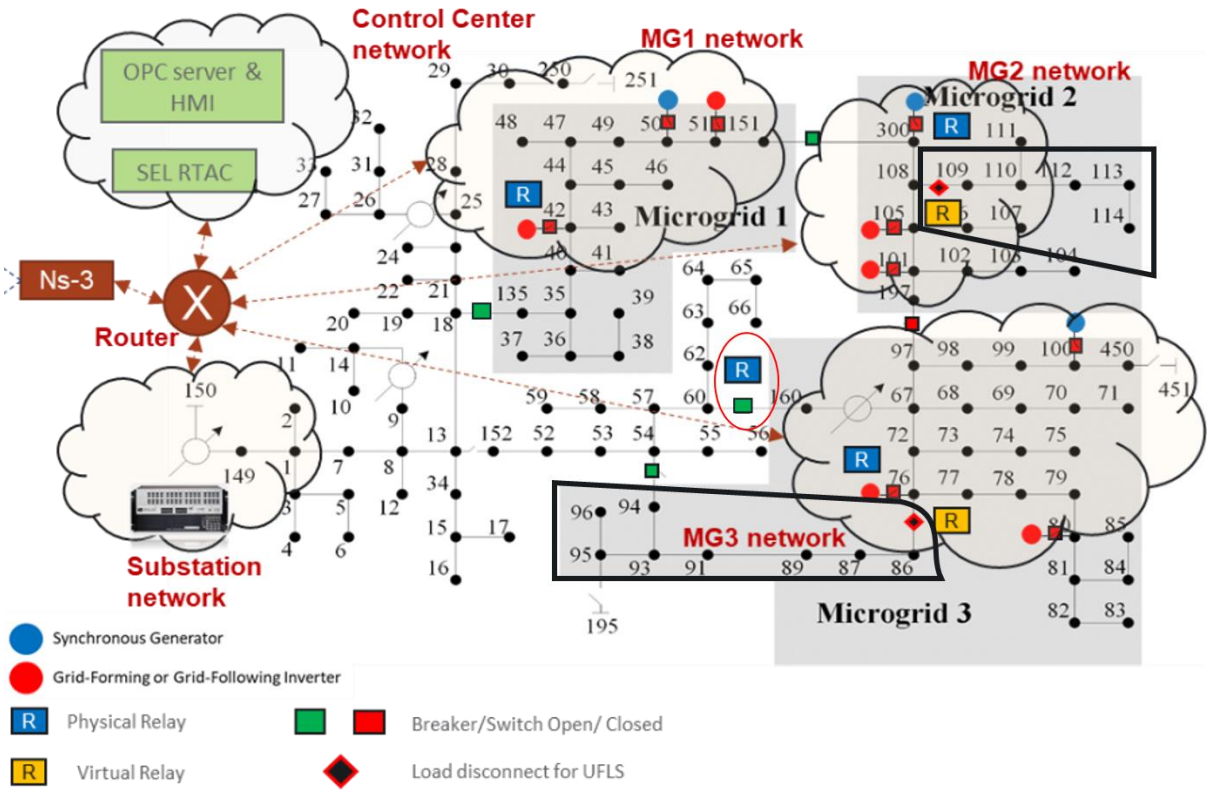

Figure 33: Scenario 6 schematic – Fully islanded implementation

7.0 Scalability for High-fidelity Experimentation

In order to understand the complex interactions between inverter-based resources, especially at higher penetrations, it is important to study the power distribution system at scale. Such studies, especially when conducted using real-time simulators can de-risk grid-enhancing investments and accelerate the adoption of newer technologies in the grid. While this makes for interesting use cases, there are challenges with maintaining high-fidelity as the model scale increases.

One of the primary challenges is managing computational burden to maintain real-time simulations as the model scale increases. The project has chosen the 9500-node test feeder, one of the largest available test feeders and the only one which provides wide variations in the adoption of newer grid-technology as the candidate model for testing scalability [31]. The 9500-node feeder (shown in Figure 34) incorporates modern feeders with enhanced smart grid technologies with legacy feeders comprising of comparable elements. Table 1 presents an overview of the computational challenges by contrasting the computational requirements for a 9500-node test feeder with the developed 123 node feeder.

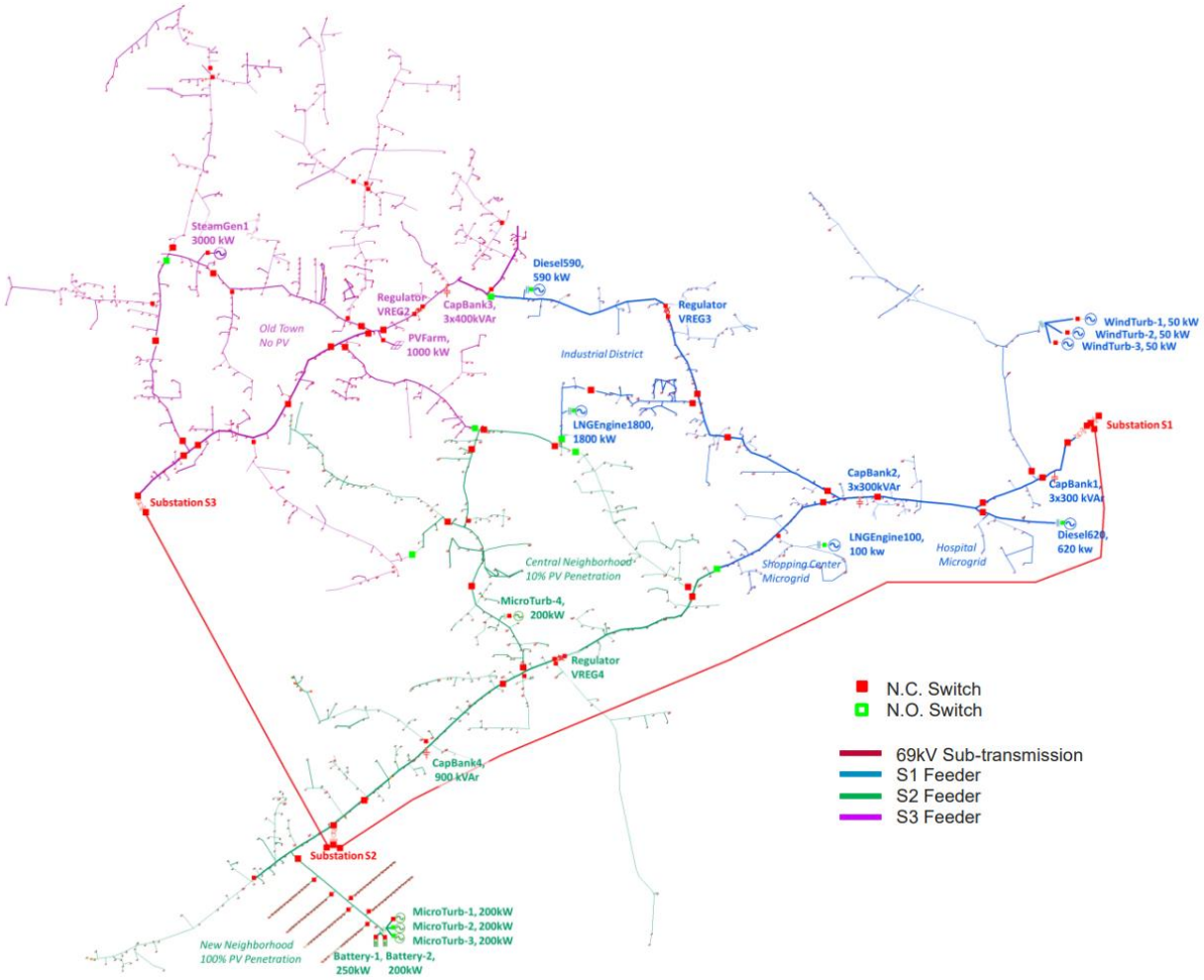

Figure 34: Topological map of the 9500-node test feeder illustrating the three main sub-feeders [31]

Number of nodes	123, 3-phase nodes (unbalanced)	9500 nodes with unbalance
Battery storage systems	0	2
Inverters	6	180 rooftop inverters
Diesel generators	3	9
Estimated CPU cores needed	8 real-time cores	32 real-time cores

Table 1: Comparison of computational burdens between the 123-node and 9500-node test feeders

It is challenging to manage the computational burden associated with simulating such systems in high-fidelity owing to the presence of extensive rooftop and utility scale solar, and multiple generation sources such as BESS microturbines, wind turbines and steam generating stations.

The second challenge is model translation and conversion. A plethora of models have been developed and validated in phasor domain packages like GridLAB-D and OpenDSS. However, converting the models to real-time EMT environments is time consuming and prone to manual error. The next sections detail the two approaches developed as part of this project to tackle these challenges.

7.1 Automated Model Building

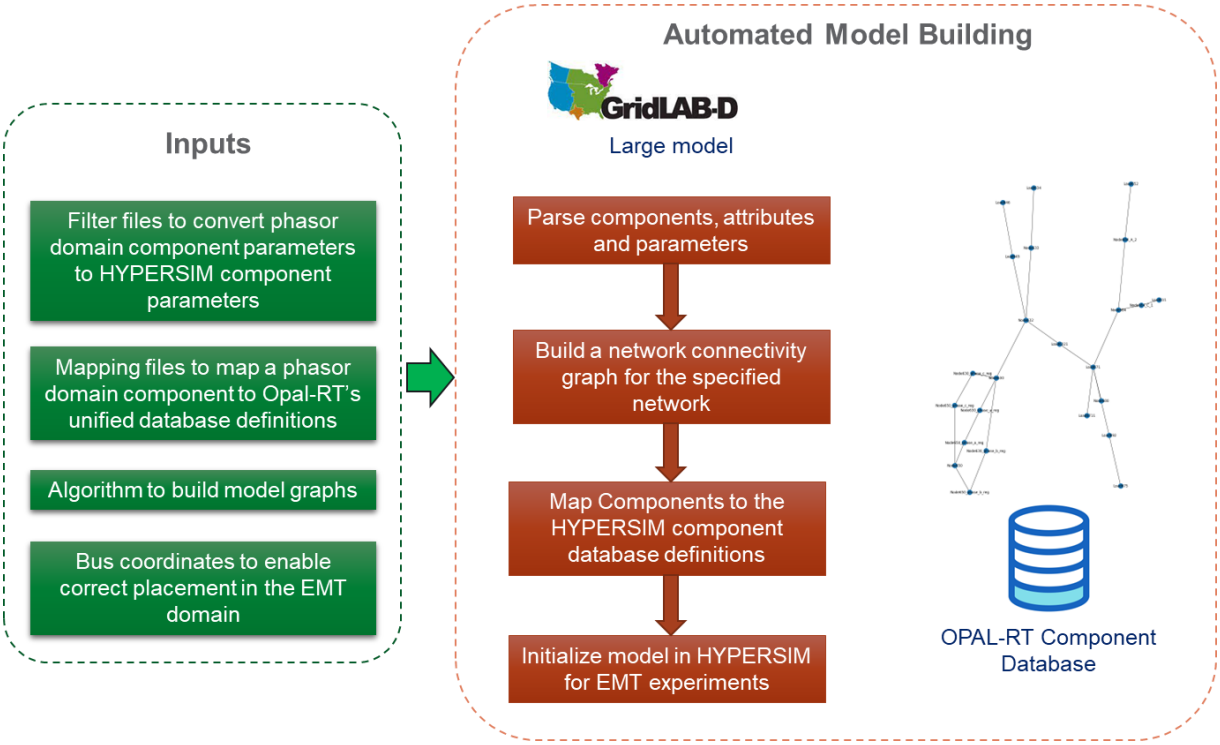

Figure 35: Automated Model Building Process

To allow the extensive library of available models in GridLAB-D to be translated and used in the real-time domain, a generic converter was built as part of this work. The converter ingests GridLAB-D models and parses all the relevant components. The components and their connectivity is then derived using scripts to construct a network graph with all the relevant attributes of the model components. A netlist of components is then constructed in a text-based format specifying dictionaries of data about buses, line parameters, transformer parameters, switch states, load definitions and other relevant parameters. A mapper is built to filter the parameters from the netlist and map the relevant parameters to the analogous components in HYPERSIM's component database. Lastly, the mapped model is initialized in HYPERSIM to translate the model into the real-time domain in the HYPERSIM user interface. Figure 35 shows a flowchart detailing these steps. Figure 36 shows a snapshot showing a converted IEEE 13 bus test feeder from the GridLAB-D format to HYPERSIM. While this enables large models to be translated to the high-fidelity domain, the challenge associated with simulating these models remains due to the computational burden.

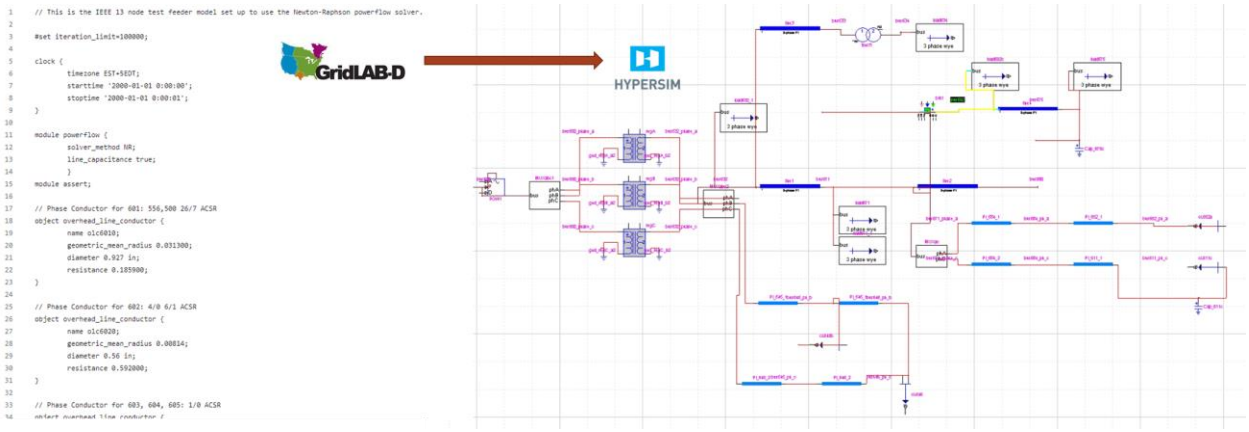

Figure 36: Conversion snapshot for an IEEE 13 bus test feeder

7.2 Multi-Fidelity Approach for Large Models

Real time simulation of large networks like the 9500-node test feeder, with many generating resources and variety of loads can be computationally challenging. One of the often-implemented solutions in such a case is model reduction. However, if the impedances between inverter-based resources are inaccurately estimated, this can give erroneous results, and the simulation studies may not reflect real-world responses. The solution utilized in this work focuses on implementing a multi-fidelity approach. The approach centers on dividing the network and co-simulating it in the phasor and EMT domain. The approach allows granular dynamics to be observed in real-time while co-simulating the rest of the system in a lower fidelity domain. Figure 37 illustrates the balance between accuracy and scale as a result of this. Small networks may be simulated in real-time on a single CPU core with high accuracy, but these approaches severely limit the achievable model scale. The approach highlighted in Section 2.2 introduces negligible errors in the system solution while allowing parallel simulation on multiple CPU cores. A multi-fidelity approach leverages all the computation power available to simulate a large portion of the network in real-time while offloading the rest of the network in the low-fidelity phasor domain at the cost of a compromise in accuracy.

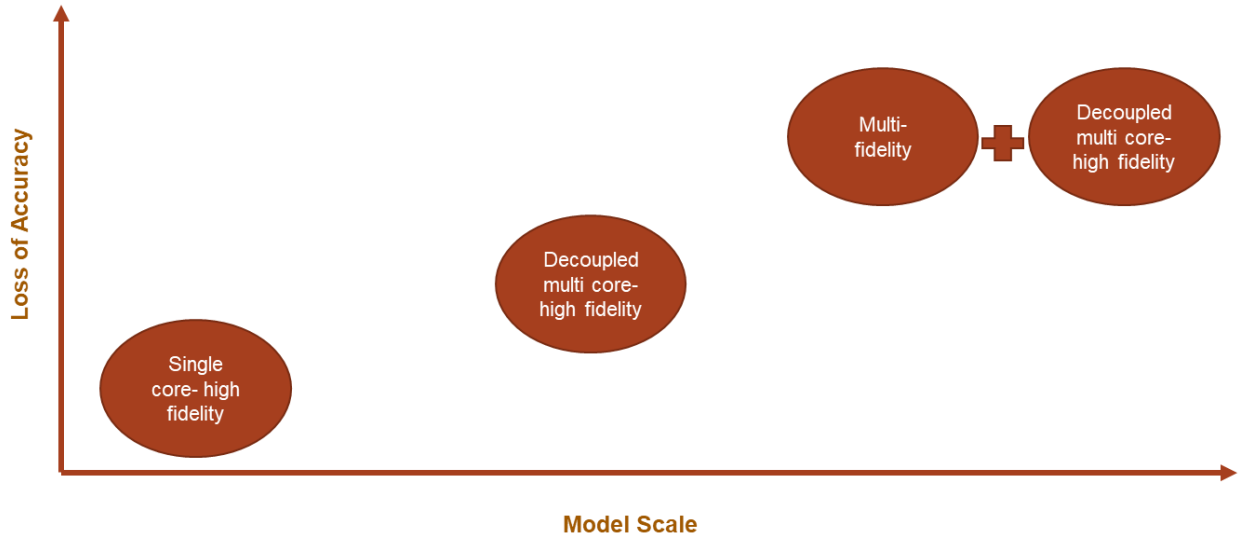

Figure 37: Compromise between accuracy and model scale for different fidelity approaches

The work implemented detailed distribution model for the 9500-node system by combining real-time simulation of parts of the grid with quasi-static time series simulation with other parts. These were integrated using the co-simulation platform HELICS. For quasi-static time series, power distribution system solver GridLAB-D was used. HYPERSIM was retained as the real-time simulator for these purposes. As an initial step, automation scripts were developed to dynamically separate large feeder networks so that part of them could be simulated in real-time, and part in quasi-static time series. This used python-based Networkx graph tool [32] to convert large feeders into graphs. These graphs had power system elements such as electric loads, nodes, generators acting as graph nodes, and power system link objects such as underground and overhead lines and transformers acting as edges. This categorization can be extended to separate any radial feeder to co-simulate it in different solvers. Two low-fidelity models are then generated for the two federates based on the boundary.

Once the feeders could be separated, the low fidelity (GridLAB-D) portion of the feeder provided the electric voltage at the point of interconnection, and the real time simulated feeder provided the total load at the point of interconnection. This could replicate a close-to real world feeder with high fidelity details modeled and simulated in real-time, while the large-scale system modeled in GridLAB-D, all interaction through the co-simulation platform. The automated model building tool detailed in Section 7.1 was utilized to convert the high-fidelity federate from GridLAB-D to HYPERSIM.

To orchestrate the co-simulation between the high-fidelity model in HYPERSIM with the large-scale quasi-static time series simulation in GridLAB-D, we utilized the HELICS middle-ware platform [33]. HELICS is an open-source co-simulation platform that was developed to operate with off-the-shelf simulators for a wide range of power system applications such as electric transmission systems, electric distribution systems, communication systems, market models, and end-use loads. HELICS facilitates data exchanges and time coordination between multi-time-scale and multi-domain simulators, the feature that is utilized in this project. HELICS provides a rich set of application programming interfaces (APIs) for other languages, including Python, C, Java, and MATLAB, which enables plugs to co-simulate the simulators that support those APIs. Figure 38 highlights the setup proposed above.

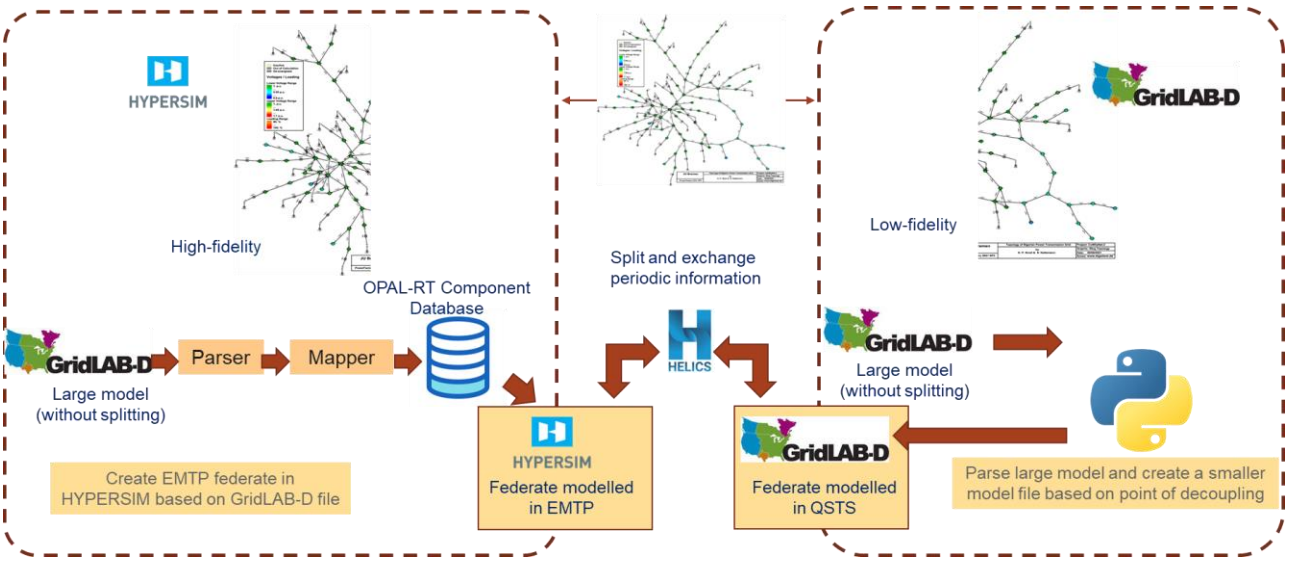

Figure 38: Multi-fidelity Setup to enable scalability.

The developed 9500 node test feeder is thereby split using the multi-fidelity approaches shown in Figure 39. The developed model will serve to enable validation and retyping of controls, mitigation strategies and analysis of system modes in more complex environments.

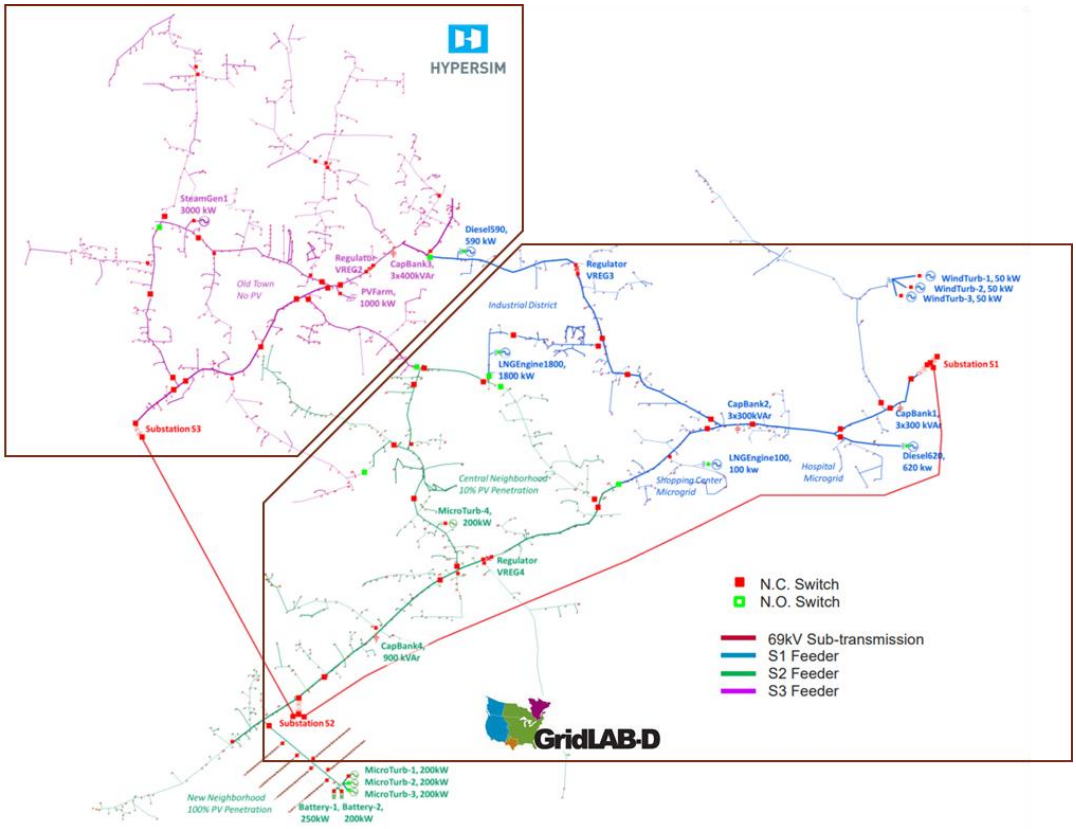

Figure 39: Multi-fidelity implementation for the IEEE 9500 node test feeder

8.0 Impact and Outcomes

Increasing penetration of DERs have introduced fast grid dynamics in traditional power systems. Reconfigurable structures like microgrids are becoming prevalent making distribution networks highly reconfigurable. To study the behavior of complex systems, it is important to understand their behavior, interactions with control schemes and assess their vulnerability to ensure safe, reliable and resilient operations in high-fidelity. Existing approaches fail to encapsulate controls, protection and communications effectively while analyzing the system at high-fidelity. The work presented in this report attempts to construct a testbed capable of allowing high-fidelity simulations in an environment where controllers, power hardware-in-the-loop, protection functions and realistic communication topologies can co-exist.

The developed testbed has been utilized generate numerous high-fidelity datasets. These datasets have found application in studies focused on defining resilience metrics, testing advanced inverter controls, defining fidelity metrics as well as identifying attack models for distribution systems. The developed orchestration pipelines have succeeded in creating an experiment methodology and process to generate exhaustive datasets to integrate and validate novel control schemes. The work had also resulted in the development of a tool that allows model translation to enable larger and more complex models to be developed. Tools allowing multi-fidelity analysis have been developed to enable computationally efficient approaches to be explored for large system simulation. Integration of the developed testbed into a transmission and distribution study has been explored to study operator responses as system conditions vary in an ancillary project. The developed experimentation platform will be leveraged effectively in future studies to understand the multimodalities and complex interdependency in distribution systems and the associated off-normal behavior that may occur.

9.0 References

[1] R. H. Lasseter et al., “CERTS Microgrid Laboratory Test Bed,” IEEE Trans. Power Deliv., vol. 26, no. 1, pp. 325–332, Jan. 2011, doi: 10.1109/TPWRD.2010.2051819.

[2] E. Limpaecher, R. Salcedo, E. Corbett, S. Manson, B. Nayak, and W. Allen, “Lessons Learned From Hardware-in-the-Loop Testing of Microgrid Control Systems,”Presented at the Grid of the Future Symposium, Oct. 2017

[3] A. Vukojevic, “Lessons learned from microgrid implementation at electric utility,” in 2018 IEEE Power & Energy Society Innovative Smart Grid Technologies Conference (ISGT), Feb. 2018, pp. 1–5. doi: 10.1109/ISGT.2018.8403338.

[4] B. Xiao et al., “Development of hardware-in-the-loop microgrid testbed,” in 2015 IEEE Energy Conversion Congress and Exposition (ECCE), Sep. 2015, pp. 1196–1202. doi: 10.1109/ECCE.2015.7309827.

[5] A. Genić, P. Gartner, D. Medjo, and M. Dinić, “Multi-layer hardware-in-the-loop testbed for microgrids,” in 2016 International Conference on Smart Systems and Technologies (SST), Oct. 2016, pp. 95–102. doi: 10.1109/SST.2016.7765640.

[6] Y. Du, H. Tu, S. Lukic, D. Lubkeman, A. Dubey, and G. Karsai, “Development of a Controller Hardware-in-the-Loop Platform for Microgrid Distributed Control Applications,” in 2018 IEEE Electronic Power Grid (eGrid), Nov. 2018, pp. 1–6. doi: 10.1109/eGRID.2018.8598696.

[7] A. Hahn, A. Ashok, S. Sridhar, and M. Govindarasu, “Cyber-Physical Security Testbeds: Architecture, Application, and Evaluation for Smart Grid,” IEEE Trans. Smart Grid, vol. 4, no. 2, pp. 847–855, Jun. 2013, doi: 10.1109/TSG.2012.2226919.

[8] “Power system simulation | Power system Analysis | HYPERSIM,” OPAL-RT. https://www.opal-rt.com/systems-hypersim/ (accessed Sep. 11, 2023).

[9] “FPGA simulator | FPGA prototyping | eFPGASIM,” OPAL-RT. https://www.opal-rt.com/systems-efpgasim/ (accessed Sep. 11, 2023).

[10] “Center for High Fidelity Science in Operational and Information Technology | PNNL.” https://www.pnnl.gov/projects/center-high-fidelity-science-operational-and-information-technology (accessed Sep. 11, 2023).

[11] “Advanced Building Controls | PNNL.” https://www.pnnl.gov/advanced-building-controls (accessed Sep. 11, 2023).

[12] “Systems Engineering Building | PNNL.” https://www.pnnl.gov/systems-engineering-building (accessed Sep. 11, 2023).

[13] “GridLAB-DTM | PNNL.” https://www.pnnl.gov/available-technologies/gridlab-dtm (accessed Sep. 11, 2023).

[14] “EMT Modelling and Simulation – Who Needs an EMT Model for Doing Stability Studies - Babak Badrzadeh (May 2022) - ESIG.” https://www.esig.energy/resources/emt-modelling-and-

simulation-who-needs-an-emt-model-for-doing-stability-studies-babak-badrzadeh-may-2022/ (accessed Sep. 11, 2023).

[15] Y. Zhang, A. M. Gole, W. Wu, B. Zhang, and H. Sun, “Development and Analysis of Applicability of a Hybrid Transient Simulation Platform Combining TSA and EMT Elements,” IEEE Trans. Power Syst., vol. 28, no. 1, pp. 357–366, Feb. 2013, doi: 10.1109/TPWRS.2012.2196450.

[16] D. Shu, X. Xie, V. Dinavahi, C. Zhang, X. Ye, and Q. Jiang, “Dynamic Phasor Based Interface Model for EMT and Transient Stability Hybrid Simulations,” IEEE Trans. Power Syst., vol. 33, no. 4, pp. 3930–3939, Jul. 2018, doi: 10.1109/TPWRS.2017.2766269.

[17] M.-E. Grenier, D. Lefebvre, and T. Van Cutsem, “Quasi steady-state models for long-term voltage and frequency dynamics simulation,” in 2005 IEEE Russia Power Tech, Jun. 2005, pp. 1–8. doi: 10.1109/PTC.2005.4524400.

[18] P. Zadkhast, X. Lin, F. Howell, B. Ko, and K. Hur, “Practical challenges in hybrid simulation studies interfacing transient stability and electro-magnetic transient simulations,” Electr. Power Syst. Res., vol. 190, p. 106596, Jan. 2021, doi: 10.1016/j.epsr.2020.106596.

[19] F. J. Plumier, C. Geuzaine, and T. Van Cutsem, “On the convergence of relaxation schemes to couple phasor-mode and electromagnetic transients simulations,” in 2014 IEEE PES General Meeting | Conference & Exposition, Jul. 2014, pp. 1–5. doi: 10.1109/PESGM.2014.6939403.

[20] C. Rehtanz and X. Guillaud, “Real-time and co-simulations for the development of power system monitoring, control and protection,” in 2016 Power Systems Computation Conference (PSCC), Jun. 2016, pp. 1–20. doi: 10.1109/PSCC.2016.7541030.

[21] “Delay-Based Decoupling of Power System Models for Transient Stability Analysis | IEEE Journals & Magazine | IEEE Xplore.” https://ieeexplore.ieee.org/document/9140373 (accessed Sep. 11, 2023).

[22] B. Ahmed, A. Abdelgadir, N. A. Saied, and A. A. Karrar, “A Compensated Distributed-Parameter Line Decoupling Approach for Real Time Applications,” IEEE Trans. Smart Grid, vol. 12, no. 2, pp. 1761–1771, Mar. 2021, doi: 10.1109/TSG.2020.3033145.

[23] R. Jinsiwale, M. Maharjan, T. Becejac, and A. Ashok, “Evaluating a real-time model decoupling compensation approach for developing scalable, high-fidelity microgrid models,” in 2023 IEEE Texas Power and Energy Conference (TPEC), Feb. 2023, pp. 1–6. doi: 10.1109/TPEC56611.2023.10078472.

[24] IEEE Power and Energy Society (PES) Analytic Methods, for Power Systems (AMPS) Distribution System Analysis, and Subcommittee, “IEEE 123 node test feeder specification.”, [Online]. Available: https://cmte.ieee.org/pes-testfeeders/resources/

[25] W. Du et al., “A Comparative Study of Two Widely Used Grid-Forming Droop Controls on Microgrid Small-Signal Stability,” IEEE J. Emerg. Sel. Top. Power Electron., vol. 8, no. 2, pp. 963–975, Jun. 2020, doi: 10.1109/JESTPE.2019.2942491.

[26] W. Du et al., “Modeling of Grid-Forming and Grid-Following Inverters for Dynamic Simulation of Large-Scale Distribution Systems,” IEEE Trans. Power Deliv., vol. 36, no. 4, pp. 2035–2045, Aug. 2021, doi: 10.1109/TPWRD.2020.3018647.

[27] “SEL-351 Protection System,” selinc.com. https://selinc.com/products/351/ (accessed Sep. 11, 2023).

[28] “Caldera.” https://caldera.mitre.org/ (accessed Sep. 11, 2023).

[29] “Search | Datahub.” https://data.pnnl.gov/ (accessed Sep. 12, 2023).

[30] Y. R. Omar, I. Z. Abidin, S. Yusof, H. Hashim, and H. A. A. Rashid, “Under frequency load shedding (UFLS): Principles and implementation,” in 2010 IEEE International Conference on Power and Energy, Nov. 2010, pp. 414–419. doi: 10.1109/PECON.2010.5697619.

[31] A. A. Anderson et al., “Introducing the 9500 Node Distribution Test System to Support Advanced Power Applications | Report | PNNL,” 2022. https://www.pnnl.gov/publications/introducing-9500-node-distribution-test-system-support-advanced-power-applications (accessed Sep. 11, 2023).

[32] “NetworkX — NetworkX documentation.” https://networkx.org/ (accessed Sep. 12, 2023).

[33] “HELICS.” https://helics.org/ (accessed Sep. 11, 2023).

Pacific Northwest National Laboratory

902 Battelle Boulevard
P.O. Box 999
Richland, WA 99354

1-888-375-PNNL (7665)

www.pnnl.gov